

A Bayesian Group Sparse Multi-Task Regression Model for Imaging Genetics

Keelin Greenlaw¹, Elena Szefer², Jinko Graham², Mary Lesperance,¹
and Farouk S. Nathoo^{1,*}

¹Department of Mathematics and Statistics, University of Victoria

²Statistics and Actuarial Science, Simon Fraser University

*nathoo@uvic.ca

October 18, 2016

Abstract

Motivation: Recent advances in technology for brain imaging and high-throughput genotyping have motivated studies examining the influence of genetic variation on brain structure. Wang et al. (*Bioinformatics*, 2012) have developed an approach for the analysis of imaging genomic studies using penalized multi-task regression with regularization based on a novel group $l_{2,1}$ -norm penalty which encourages structured sparsity at both the gene level and SNP level. While incorporating a number of useful features, the proposed method only furnishes a point estimate of the regression coefficients; techniques for conducting statistical inference are not provided. A new Bayesian method is proposed here to overcome this limitation.

Results: We develop a Bayesian hierarchical modeling formulation where the posterior mode corresponds to the estimator proposed by Wang et al. (*Bioinformatics*, 2012), and an approach that allows for full posterior inference including the construction of interval estimates for the regression parameters. We show that the proposed hierarchical model can be expressed as a three-level Gaussian scale mixture and this representation facilitates the use of a Gibbs sampling algorithm for posterior simulation. Simulation studies demonstrate that the interval estimates obtained using our approach achieve adequate coverage probabilities that outperform those obtained from the nonparametric bootstrap. Our proposed methodology is applied to the analysis of neuroimaging and genetic data collected as part of the Alzheimer's Disease Neuroimaging Initiative (ADNI), and this analysis of the ADNI cohort demonstrates clearly the value added of incorporating interval estimation beyond only point estimation when relating SNPs to brain imaging endophenotypes. Software is publicly available at <https://cran.r-project.org/web/packages/bgsmtr/index.html>.

1 Introduction

Imaging genetics involves the use of structural or functional neuroimaging data to study subjects carrying genetic risk variants that may relate to neurological disorders such as Alzheimer’s disease. In such studies the primary interest lies with examining associations between genetic variations and neuroimaging measures which represent quantitative traits. Compared to studies examining more traditional phenotypes such as case-control status, the endophenotypes derived through neuroimaging are in some cases considered closer to the underlying etiology of the disease being studied, and this may lead to easier identification of the important genetic variations. A number of settings for statistical analysis in imaging genetics have been studied involving different combinations of gene versus genome-wide and region of interest (ROI) versus image-wide analysis, all of which have different advantages and limitations as discussed in Ge et al. (2013).

The earliest methods developed for imaging genomics data analysis are either based on significant reductions to both data types or they employ full brain-wide genome-wide scans based on a massive number of pairwise univariate analyses (e.g. Stein et al., 2010). While these approaches are convenient in terms of their implementation they ignore potential multicollinearity arising from variants within the same LD block, and they also ignore the potential relationship between the different neuroimaging endophenotypes. Ignoring these relationships precludes the borrowing of information about the genetic associations across components of the response vector. Hibar et al. (2011) use gene-based multi-variate statistics and avoid having collinearity of SNP vectors by using dimensionality reduction. Vounou et al. (2010) develop a sparse reduced-rank regression approach for studies involving high-dimensional neuroimaging phenotypes, while Ge et al. (2012) develop a flexible multi-locus approach based on least squares kernel machines. In the latter case, the authors employ permutation testing procedures and take advantage of the spatial information inherent in brain images by using random field theory as an inferential tool (Worsley, 2002). More recently, Stingo et al. (2013) develop a Bayesian hierarchical mixture model for relating brain connectivity to genetic information for studies involving functional magnetic resonance imaging (fMRI) data. The mixture components of the proposed model correspond to the classification of the study subjects into subgroups, and the allocation of subjects to these mixture components is linked to genetic covariates with regression parameters assigned spike-and-slab priors. The proposed model is used to examine the relationship between functional brain connectivity based on fMRI data and genetic variation.

In contrast, the focus of our work concerns the development of methodology for studies where the neuroimaging phenotypes consist of volumetric and cortical thickness measures derived from MRI which summarize the structure (as opposed to the function) of the brain over a relatively moderate number (e.g. up to 100) ROI’s, and we are interested in relating brain structure to genetics.

We develop a Bayesian approach based on a continuous shrinkage prior that encourages sparsity and induces dependence in the regression coefficients corresponding to SNPs within the same gene, and across different components of the imaging phenotypes. Our approach is related to the Bayesian group lasso (Park and Casella, 2008; Kyung et al., 2010) but it is

adapted to accommodate multivariate phenotypes and it is extended to allow for grouping penalties both at the gene and SNP level. Our work is primarily motivated by the recent work of Wang et al. (2012) who propose an estimator based on group sparse regularization applied to multivariate regression where SNPs are grouped by genes or LD blocks. In what follows we will assume for specificity that the groups correspond to genes; however, this assumption is not necessary and any approach for grouping the SNPs (e.g. LD blocks) may be used. Let $\mathbf{y}_\ell = (y_{\ell 1}, \dots, y_{\ell c})^T$ denote the imaging phenotype summarizing the structure of the brain over c ROIs for subject ℓ , $\ell = 1, \dots, n$. The corresponding genetic data are denoted by $\mathbf{x}_\ell = (x_{\ell 1}, \dots, x_{\ell d})^T$, $\ell = 1, \dots, n$, where we have information on d SNPs, and $x_{\ell j} \in \{0, 1, 2\}$ is the number of minor alleles for the j^{th} SNP. We further assume that the set of SNPs can be partitioned into K groups, for example K genes, and we let $\pi_k, k = 1, 2, \dots, K$, denote the set containing the SNP indices corresponding to the k^{th} group and $m_k = |\pi_k|$. We assume that $E(\mathbf{y}_\ell) = \mathbf{W}^T \mathbf{x}_\ell$, $\ell = 1, \dots, n$, where \mathbf{W} is a $d \times c$ matrix, with each row characterizing the association between a given SNP and the brain summary measures across all ROIs. The estimator proposed by Wang et al. (2012) takes the form

$$\hat{\mathbf{W}} = \arg \min_{\mathbf{W}} \sum_{\ell=1}^n \|\mathbf{W}^T \mathbf{x}_\ell - \mathbf{y}_\ell\|_2^2 + \gamma_1 \|\mathbf{W}\|_{G_{2,1}} + \gamma_2 \|\mathbf{W}\|_{l_{2,1}} \quad (1)$$

where γ_1 and γ_2 are regularization parameters weighting a $G_{2,1}$ -norm penalty $\|\mathbf{W}\|_{G_{2,1}} = \sum_{k=1}^K \sqrt{\sum_{i \in \pi_k} \sum_{j=1}^c w_{ij}^2}$ and an $l_{2,1}$ -norm penalty $\|\mathbf{W}\|_{l_{2,1}} = \sum_{i=1}^d \sqrt{\sum_{j=1}^c w_{ij}^2}$ respectively. The $G_{2,1}$ -norm addresses group-wise association between SNPs and encourages sparsity at the gene level. This regularization differs from group lasso (Yuan and Lin, 2006) as it penalizes regression coefficients for a group of SNPs across all imaging phenotypes jointly. As an important gene/group may contain irrelevant individual SNPs, or a less important group may contain individually significant SNPs, the second penalty, an $l_{2,1}$ -norm (Evgeniou and Pontil, 2007), is added to allow for additional structured sparsity.

The estimator (1) provides a novel approach for assessing associations between neuroimaging phenotypes and genetic variations as it accounts for several interrelated structures within genotyping and imaging data. The incorporation of biological group structure in regression analysis with genetic data has been developed in a variety of contexts (see e.g. Stingo et al., 2011; Wen, 2014; Rockova et al., 2014; Zhu et al., 2014). Wang et al. (2012) show that such an approach when applied to imaging genetics is able to achieve enhanced predictive performance and improved SNP selection compared with a number of alternative approaches in certain settings. Notwithstanding these advantages, a limitation of the proposed methodology is that it only furnishes a point estimate $\hat{\mathbf{W}}$ and techniques for obtaining valid standard errors or interval estimates are not provided. The primary contribution of this article is to provide an approach for doing this.

Resampling methods such as the bootstrap are a natural starting point for this problem; however, as discussed in Kyung et al. (2010) the bootstrap estimates of the standard error for the lasso or lasso variations such as the estimator (1) might be unstable and not perform well. An alternative way forward is to exploit the connection between penalized regression methods and hierarchical modeling formulations. Following the ideas of Park and Casella

(2008) and Kyung et al. (2010) we develop a hierarchical Bayesian model that allows for full posterior inference. The spread of the posterior distribution then provides valid measures of posterior variability along with credible intervals for each regression parameter. Along similar lines, Bae and Mallick (2004) develop a two-level hierarchical model for gene selection that incorporates the univariate Laplace distribution as a prior that favors sparsity and employ the representation of the Laplace distribution as a Gaussian scale mixture in their model hierarchy. In our work, we use a multivariate prior based on a Gaussian scale mixture representation which is assigned independently to the set of coefficients corresponding to each gene. The prior is chosen so that the corresponding posterior mode is exactly the Wang et al. (2012) estimator. To our knowledge this specific form of multivariate shrinkage prior has not been considered previously, though the formulation is related to the general ideas developed in Kyung et al. (2010).

The remainder of the paper proceeds as follows. In Section 2 we specify the hierarchical model and its motivation based on the estimator (1). The scale mixture representation is specified and a Gibbs sampling algorithm for computing the posterior distribution is presented. Section 3 presents a study of computation time and scaling, while simulation studies are presented in Section 4. Section 5 applies our methodology to a dataset obtained from the Alzheimer’s Disease Neuroimaging Initiative (ADNI) database, where we relate MRI based structural brain summaries at 56 ROIs to 486 SNPs belonging to 33 genes. The final section concludes with a discussion of potential model extensions.

2 Methods

Let $\mathbf{W}^{(k)} = (w_{ij})_{i \in \pi_k}$ denote the $m_k \times c$ submatrix of \mathbf{W} containing the rows corresponding to the k^{th} gene, $k = 1, \dots, K$. The hierarchical model corresponding to the estimator (1) takes the form

$$\mathbf{y}_\ell | \mathbf{W}, \sigma^2 \stackrel{ind}{\sim} MVN_c(\mathbf{W}^T \mathbf{x}_\ell, \sigma^2 I_c) \quad \ell = 1, \dots, n, \quad (2)$$

with the coefficients corresponding to different genes assumed conditionally independent

$$\mathbf{W}^{(k)} | \lambda_1^2, \lambda_2^2, \sigma^2 \stackrel{ind}{\sim} p(\mathbf{W}^{(k)} | \lambda_1^2, \lambda_2^2, \sigma^2) \quad k = 1, \dots, K, \quad (3)$$

and with the prior distribution for each $\mathbf{W}^{(k)}$ having a density function given by

$$p(\mathbf{W}^{(k)} | \lambda_1^2, \lambda_2^2, \sigma^2) \propto \exp \left\{ -\frac{\lambda_1}{\sigma} \sqrt{\sum_{i \in \pi_k} \sum_{j=1}^c w_{ij}^2} \right\} \\ \times \prod_{i \in \pi_k} \exp \left\{ -\frac{\lambda_2}{\sigma} \sqrt{\sum_{j=1}^c w_{ij}^2} \right\}. \quad (4)$$

The shrinkage prior (4) is not a multivariate Laplace distribution; however, each term of the product on the right-hand side of (4) is the kernel of a form of the multivariate Laplace

distribution discussed in Kotz et al. (2001), and so we refer to this prior as the *product multivariate Laplace distribution*. The prior is specified conditional on σ and the dependence of the prior density on σ follows the parameterization of the univariate Laplace distribution considered in Park and Casella (2008) who show that this parameterization guarantees a unimodal posterior for the Bayesian lasso. By construction, the posterior mode, conditional on $\lambda_1^2, \lambda_2^2, \sigma^2$, corresponding to the model hierarchy (2) - (4) is exactly the estimator (1) proposed by Wang et al. (2012) with $\gamma_1 = 2\sigma\lambda_1$ and $\gamma_2 = 2\sigma\lambda_2$. This equivalence between the posterior mode and the estimator of Wang et al. (2012) is the motivation for our model; however, we note that generalizations that allow for a more flexible covariance structure in (2) could also be considered. For the current model each component of \mathbf{y}_ℓ is scaled to have unit variance across subjects, making the assumption of a single variance component σ^2 tenable. We also note that while (2) assumes conditional independence across imaging phenotypes, the prior distribution (4) induces dependence in the regression coefficients across the imaging phenotypes for coefficients corresponding to the same gene (group).

PROPOSITION 1. (Prior Propriety) *The prior for \mathbf{W} based on (3) and (4) is proper.*

Proof: For each $k \in \{1, \dots, K\}$ we define I_k as

$$I_k = \int \exp \left\{ -\frac{\lambda_1}{\sigma} \sqrt{\sum_{i \in \pi_k} \sum_{j=1}^c w_{ij}^2} \right\} \\ \times \prod_{i \in \pi_k} \exp \left\{ -\frac{\lambda_2}{\sigma} \sqrt{\sum_{j=1}^c w_{ij}^2} \right\} d\mathbf{W}^{(k)}.$$

It is sufficient to show that $\prod_{k=1}^K I_k$ is finite. We note that

$$I_k \leq \int \exp \left\{ -\frac{\lambda_1}{\sigma} \sqrt{\sum_{i \in \pi_k} \sum_{j=1}^c w_{ij}^2} \right\} d\mathbf{W}^{(k)} \quad (5)$$

since $\exp(-x) \leq 1$ for $x \geq 0$. The integrand on the right-hand-side of (5) is proportional to the probability density function of a particular form of the multivariate Laplace distribution discussed in Kotz et al. (2001). Given this form, the integral can be evaluated as

$$\int \exp \left\{ -\frac{\lambda_1}{\sigma} \sqrt{\sum_{i \in \pi_k} \sum_{j=1}^c w_{ij}^2} \right\} d\mathbf{W}^{(k)} = \pi^{(m_k c - 1)/2} \\ \times \Gamma((m_k c + 1)/2) 2^{m_k c} (\lambda_1^2 / \sigma^2)^{-m_k c / 2} < \infty,$$

so that $I_k < \infty$ and therefore $\prod_{k=1}^K I_k < \infty$ as required.

If the hyper-parameters σ^2 , λ_1 , and λ_2 are fixed or assigned proper priors then Proposition 1 is sufficient to ensure that the posterior distribution is proper. The following proposition provides a stochastic representation of the prior based on a Gaussian scale mixture. This representation is important as it facilitates computation of the posterior distribution using a simple Gibbs sampling algorithm.

PROPOSITION 2. (Scale mixture representation) *For each $i \in \{1, \dots, d\}$ let $k(i) \in \{1, \dots, K\}$ denote the gene associated with the i^{th} SNP. The prior (4) can be obtained through the following scale mixture representation:*

$$w_{ij} \mid \sigma^2, \boldsymbol{\tau}^2, \boldsymbol{\omega}^2 \stackrel{\text{ind}}{\sim} N \left(0, \sigma^2 \left(\frac{1}{\tau_{k(i)}^2} + \frac{1}{\omega_i^2} \right)^{-1} \right), \quad (6)$$

with continuous scale mixing variables $\boldsymbol{\tau}^2 = (\tau_1^2, \dots, \tau_K^2)'$ and $\boldsymbol{\omega}^2 = (\omega_1^2, \dots, \omega_d^2)'$ distributed according to the density

$$\begin{aligned} & p(\boldsymbol{\tau}^2, \boldsymbol{\omega}^2 \mid \lambda_1^2, \lambda_2^2) \\ & \propto \prod_{k=1}^K \left(\frac{\lambda_1^2}{2} \right)^{\binom{m_k c + 1}{2}} (\tau_k^2)^{\binom{m_k c + 1}{2} - 1} \exp \left\{ - \left(\frac{\lambda_1^2}{2} \right) \tau_k^2 \right\} \\ & \times \prod_{i \in \pi_k} \left(\frac{\lambda_2^2}{2} \right)^{\binom{c+1}{2}} (\omega_i^2)^{\binom{c+1}{2} - 1} \exp \left\{ - \left(\frac{\lambda_2^2}{2} \right) \omega_i^2 \right\} \\ & \times (\tau_k^2 + \omega_i^2)^{-\frac{c}{2}}. \end{aligned} \quad (7)$$

Proof: From Kyung et al. (2010, Appendix 2) we have the following:

$$\begin{aligned} & \exp \left\{ - \frac{\lambda_1}{\sigma} \|\mathbf{W}^{(k)}\|_2 \right\} \propto \int_0^\infty \left(\frac{1}{2\pi\sigma^2\tau_k^2} \right)^{\frac{m_k c}{2}} \\ & \times \exp \left\{ - \frac{\|\mathbf{W}^{(k)}\|_2^2}{2\sigma^2\tau_k^2} \right\} \frac{\left(\frac{\lambda_1^2}{2} \right)^{\binom{m_k c + 1}{2}}}{\Gamma \left(\frac{m_k c + 1}{2} \right)} (\tau_k^2)^{\binom{m_k c + 1}{2} - 1} \\ & \times \exp \left\{ - \left(\frac{\lambda_1^2}{2} \right) \tau_k^2 \right\} d\tau_k^2, \end{aligned} \quad (8)$$

and

$$\begin{aligned} & \exp \left\{ - \frac{\lambda_2}{\sigma} \|\mathbf{w}^i\|_2 \right\} \propto \int_0^\infty \left(\frac{1}{2\pi\sigma^2\omega_i^2} \right)^{\frac{c}{2}} \exp \left\{ - \frac{\|\mathbf{w}^i\|_2^2}{2\sigma^2\omega_i^2} \right\} \\ & \times \frac{\left(\frac{\lambda_2^2}{2} \right)^{\binom{c+1}{2}}}{\Gamma \left(\frac{c+1}{2} \right)} (\omega_i^2)^{\binom{c+1}{2} - 1} \exp \left\{ - \left(\frac{\lambda_2^2}{2} \right) \omega_i^2 \right\} d\omega_i^2, \end{aligned} \quad (9)$$

where \mathbf{w}^i denotes the i^{th} row of \mathbf{W} . Beginning with (4) we substitute (8) and (9), apply some algebra, and simplify to obtain $p(\mathbf{W}^{(k)}|\lambda_1^2, \lambda_2^2, \sigma^2)$

$$\begin{aligned} & \propto \int_0^\infty \cdots \int_0^\infty \prod_{i \in \pi_k} \left[\left(\sigma^2 \left(\frac{1}{\tau_k^2} + \frac{1}{\omega_i^2} \right)^{-1} \right)^{-\frac{c}{2}} \right] \\ & \times \exp \left\{ - \sum_{i \in \pi_k} \left(\frac{\sum_{j=1}^c w_{ij}^2}{2 \sigma^2 \left(\frac{1}{\tau_k^2} + \frac{1}{\omega_i^2} \right)^{-1}} \right) \right\} \exp \left\{ - \frac{\lambda_1^2}{2} \tau_k^2 \right\} \\ & \times \left[\prod_{i \in \pi_k} \left(\sigma^2 \left(\frac{1}{\tau_k^2} + \frac{1}{\omega_i^2} \right)^{-1} \right)^{\frac{c}{2}} \right] \times \left(\frac{\lambda_1^2}{2} \right)^{\left(\frac{m_k c + 1}{2} \right)} (\tau_k^2)^{-\frac{1}{2}} \\ & \times \left[\prod_{i \in \pi_k} \left(\frac{\lambda_2^2}{2} \right)^{\left(\frac{c+1}{2} \right)} (\omega_i^2)^{-\frac{1}{2}} \exp \left\{ - \frac{\lambda_2^2}{2} \omega_i^2 \right\} d\omega_i^2 \right] d\tau_k^2 \end{aligned}$$

From (3), we are able to take the product of the expression above over $k \in \{1, \dots, K\}$, and after simplification we obtain $p(\mathbf{W}|\lambda_1^2, \lambda_2^2, \sigma^2)$

$$\begin{aligned} & \propto \int_0^\infty \cdots \int_0^\infty \prod_{k=1}^K \prod_{i \in \pi_k} N(w_{ij}; 0, \sigma^2 \left(\frac{1}{\tau_k^2} + \frac{1}{\omega_i^2} \right)^{-1}) \\ & \times \prod_{k=1}^K \left(\frac{\lambda_1^2}{2} \right)^{\left(\frac{m_k c + 1}{2} \right)} (\tau_k^2)^{\frac{m_k c + 1}{2} - 1} \exp \left\{ - \frac{\lambda_1^2}{2} \tau_k^2 \right\} \\ & \times \left[\prod_{i \in \pi_k} \left(\frac{\lambda_2^2}{2} \right)^{\left(\frac{c+1}{2} \right)} (\omega_i^2)^{\frac{c+1}{2} - 1} \exp \left\{ - \frac{\lambda_2^2}{2} \omega_i^2 \right\} \right] \\ & \times \left[\prod_{i \in \pi_k} (\tau_k^2 + \omega_i^2)^{-\frac{c}{2}} d\omega_i^2 \right] d\tau_k^2, \end{aligned} \tag{10}$$

where $N(x; \mu, \sigma^2)$ denotes the density of a normal distribution with mean μ , variance σ^2 evaluated at x . The first line of the integrand in (10) corresponds to (6), while the remaining lines of (10) correspond to (7), and the integration is over the scale mixing variables $\boldsymbol{\tau}^2$ and $\boldsymbol{\omega}^2$. It follows that (3)-(4) can be represented through the Gaussian scale mixture (6)-(7).

This hierarchical representation of the shrinkage prior (7) introduces gene specific latent variables $\tau_1^2, \dots, \tau_K^2$ as well as SNP specific latent variables $\omega_1^2, \dots, \omega_d^2$ that modulate the conditional variance of each regression coefficient in (6). Unlike other formulations for Bayesian lassos the scale mixing variables are not assumed independent. The dependence in the joint distribution arises from the term $(\tau_k^2 + \omega_i^2)^{-\frac{c}{2}}$ in (7) and this is required to ensure

that the resulting marginal distribution for \mathbf{W} has the required form (4). The parameter σ^2 is assigned a proper inverse-Gamma prior

$$\sigma^2 \sim \text{Inv} - \text{Gamma}(a_\sigma, b_\sigma), \quad (11)$$

and the hierarchical model (2), (6), (7), and (11) has a conjugacy structure that facilitates posterior simulation using a Gibbs sampling algorithm. As the normalizing constant associated with (7) is not known and may not exist, we work with the unnormalized form which yields proper full conditional distributions having standard form. Our focus of inference does not lie with the scale mixing variables themselves, rather, the use of the scale mixture representation is a computational device that leads to a fairly straightforward Gibbs sampling algorithm which enables us to draw from the marginal posterior of \mathbf{W} . By Proposition 1 and the fact that (11) is proper we are assured that this posterior distribution is always proper. The Gibbs sampler is presented in Algorithm 1 while the corresponding derivations are presented in the supplementary material. Starting values for the algorithm can be obtained in part by first computing the estimator (1) and using these to initialize the MCMC sampler.

Algorithm 1 Gibbs Sampling Algorithm

1. Set tuning parameters λ_1^2 and λ_2^2 .
2. Initialize \mathbf{W} , τ^2 , ω^2 and repeat steps (3) - (6) below to obtain the desired Monte Carlo sample size after burn-in.
3. Update $\sigma^2 \sim \text{Inv-Gamma}(a_\sigma^*, b_\sigma^*)$, $a_\sigma^* = \frac{c}{2}(n + d) + a_\sigma$

$$b_\sigma^* = \frac{1}{2} \sum_{\ell=1}^n \|\mathbf{y}_\ell - \mathbf{W}^T \mathbf{x}_\ell\|_2^2 + \frac{1}{2} \sum_{i=1}^d \left(\frac{1}{\tau_{k(i)}^2} + \frac{1}{\omega_i^2} \right) \sum_{j=1}^c w_{ij}^2 + b_\sigma.$$

4. For $k = 1, \dots, K$ update τ_k^2 , through
 $1/\tau_k^2 \sim \text{Inverse-Gaussian}\left(\sqrt{\frac{\lambda_1^2 \sigma^2}{\|\mathbf{W}^{(k)}\|_F^2}}, \lambda_1^2\right).$
5. For $i = 1, \dots, d$ update ω_i^2 , through
 $1/\omega_i^2 \sim \text{Inverse-Gaussian}\left(\sqrt{\frac{\lambda_2^2 \sigma^2}{\sum_{j=1}^c w_{ij}^2}}, \lambda_2^2\right).$
6. For $k = 1, \dots, K$ update $\mathbf{W}^{(k)}$, based on
 $\text{vec}(\mathbf{W}^{(k)'}) \sim \text{MVN}_{m_k c}(\boldsymbol{\mu}_k, \boldsymbol{\Sigma}_k)$ where

$$\begin{aligned} \boldsymbol{\mu}_k &= -\mathbf{A}_k^{-1} \sum_{\ell=1}^n (\mathbf{x}_\ell^{(k)} \otimes \mathbf{I}_c) (\mathbf{x}_\ell^{(-k)'} \otimes \mathbf{I}_c) \text{vec}(\mathbf{W}^{(-k)'}) \\ &+ \mathbf{A}_k^{-1} \sum_{\ell=1}^n (\mathbf{x}_\ell^{(k)} \otimes \mathbf{I}_c) \mathbf{y}_\ell, \quad \boldsymbol{\Sigma}_k = \sigma^2 \mathbf{A}_k^{-1}, \quad \mathbf{A}_k = \\ &\sum_{\ell=1}^n (\mathbf{x}_\ell^{(k)} \otimes \mathbf{I}_c) (\mathbf{x}_\ell^{(k)'} \otimes \mathbf{I}_c) + \text{Diag}\left\{ \frac{1}{\tau_k^2} + \frac{1}{\omega_i^2} \right\}_{i \in \pi_k} \otimes \mathbf{I}_c \end{aligned}$$

and where $\mathbf{W}^{(-k)} = (w_{ij})_{i \notin \pi_k, j}$, $\mathbf{x}_\ell^{(k)} = (x_{\ell j})_{j \in \pi_k}$,
 and $\mathbf{x}_\ell^{(-k)} = (x_{\ell j})_{j \notin \pi_k}$.

The tuning parameters γ_1 , γ_2 in (1) and λ_1^2 , λ_2^2 in the hierarchical model (2), (6), (7), and (11) control the strength of the regularization terms and thus the structure of the penalty that governs the bias-variance tradeoff associated with the estimator of \mathbf{W} . Wang et al. (2012) suggest the use of five-fold cross-validation (CV) over a discrete two-dimensional grid $\{10^{-5}, 10^{-4}, \dots, 10^4, 10^5\}^2$ of possible values. A problem with the use of CV when MCMC runs are required to fit the model is that an extremely large number of parallel runs are needed to cover all points on the grid for each possible split of the data. To avoid some of this computational burden we approximate leave-one-subject-out CV using the WAIC

(Watanabe, 2010; Gelman et al., 2014)

$$\begin{aligned}
 WAIC &= -2 \sum_{l=1}^n \log E_{\mathbf{W}, \sigma^2} [p(\mathbf{y}_l | \mathbf{W}, \sigma^2) | \mathbf{y}_1, \dots, \mathbf{y}_n] \\
 &+ 2 \sum_{l=1}^n VAR_{\mathbf{W}, \sigma^2} [\log p(\mathbf{y}_l | \mathbf{W}, \sigma^2) | \mathbf{y}_1, \dots, \mathbf{y}_n]
 \end{aligned}$$

where $p(\mathbf{y}_l | \mathbf{W}, \sigma^2)$ is the probability density function associated with (2) and the required posterior means and variances are approximated based on the output of the MCMC sampler at each point of the grid. These samplers are run in parallel using a high performance computing cluster. The values of λ_1^2 and λ_2^2 are then chosen as those values that minimize the WAIC across the grid and no data-splitting is required. We note that alternative approaches based on either empirical Bayes (EB) or hierarchical Bayes (HB) could also be used to choose the tuning parameters; however, for the model under consideration we have found (Nathoo et al., 2016) that using both EB and HB to select the tuning parameters can lead to severe over-shrinkage of the posterior mean of the regression coefficients when $d > n$ or when the genetic effects are weak.

3 Computation Time and Scaling

In this section we report on computation times and scaling as the number of subjects n , the dimension of the phenotype c , and the number of SNPs d changes. Three experiments are performed with each examining how the computation time scales with one of the three input dimensions. The computation times reported here are based on a total of 10,000 MCMC iterations (5,000 iterations was a sufficient burn-in in all cases considered) with each run employing 49 cores (each 2.66-GHz Xeon x5650) on a computing cluster with 20GB of RAM requested for each job. To be clear on the parallel aspect of the computing, each core is simply used to run the Gibbs sampler with a different value of $(\lambda_1^2, \lambda_2^2)$ and the value minimizing the WAIC is used for inference in each case. The computational algorithm itself runs on a single core. When multiple cores are not available, our R package 'bgsmttr' provides alternative approaches for choosing the tuning parameters with computations using only a single core.

We choose baseline values of $c = 12$, $d = 500$, $n = 600$, and in each of the three experiments the data are simulated from the model with one dimension varying while the other two are fixed at the baseline values. The results from the three experiments are displayed in Figure 1 and Figure 2. In each case the computation time scales approximately linearly with the given input. For a fully Bayesian approach with implementation based on MCMC, the computation time is not extensive even for the most extreme values ($d = 5,000$, $c = 100$, $n = 10,000$) and larger values can be considered if more memory is available, or alternatively, thinning can be applied to the MCMC chains to reduce the memory requirements.

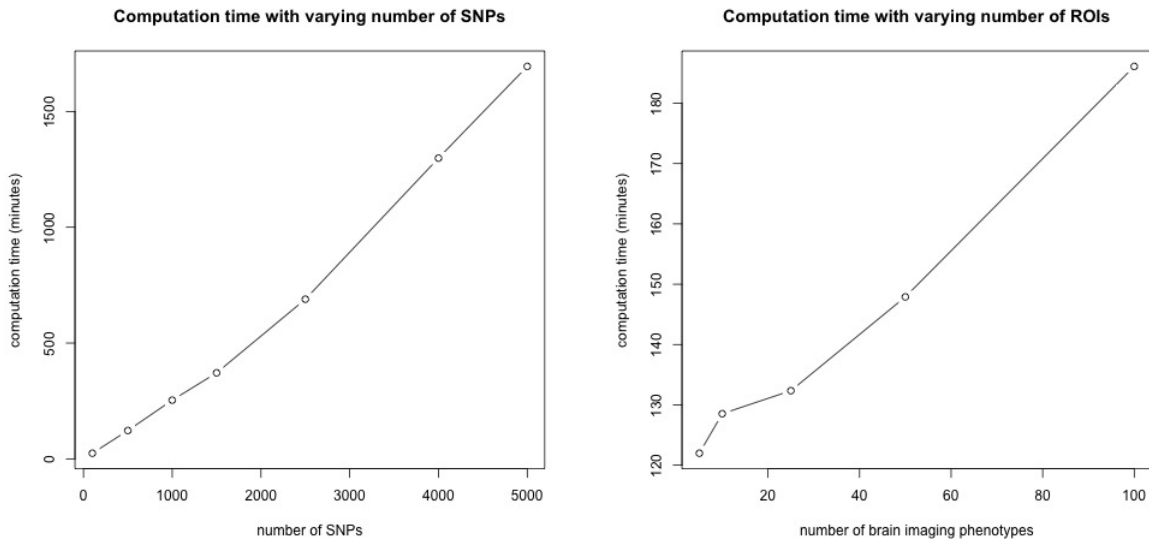


Figure 1: Computation time in minutes as a function of the number of SNPs d ($c = 12$, $n = 600$) and the number of phenotypes c ($d = 500$, $n = 600$).

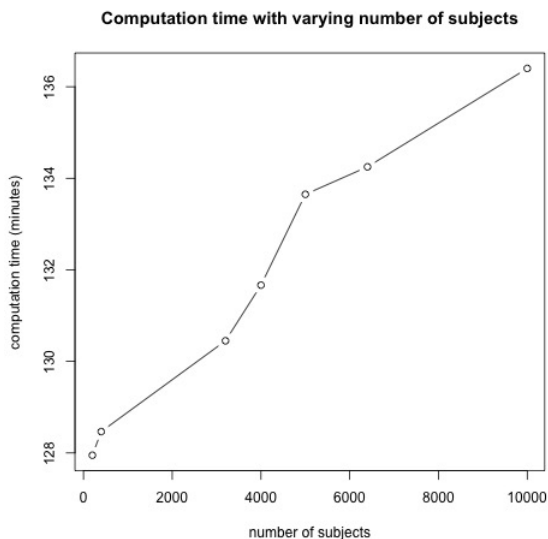


Figure 2: Computation time as a function of the number of subjects n ($c = 12$, $d = 500$).

4 Simulation Studies

We conduct four simulation studies in which our proposed methodology is evaluated with the primary objective of evaluating the coverage probabilities of the 95% equal-tail credible intervals for the regression coefficients \mathbf{W} . We focus on evaluating coverage probabilities as the ability to quantify uncertainty through interval estimation is the primary value-added

of our methodology over and above the estimator proposed by Wang et al. (2012). We also compare our approach to a more standard approach, the nonparametric bootstrap applied to the estimator (1).

The application of the nonparametric bootstrap involves resampling the data with replacement and recomputing the estimator (1) for each bootstrap sample. The bootstrap distribution of the resulting estimators over a large number $B = 1000$ bootstrap samples is then used to construct approximate 95% confidence intervals. In this case the bootstrap resampling is done at the level of subjects. The tuning parameters γ_1 and γ_2 are recomputed for each simulated dataset in the simulation study but they are fixed across all bootstrap replicates corresponding to a single simulated dataset. The selection for these tuning parameters is based on five-fold CV.

The simulation studies are based on genetic data obtained from the ADNI database. The data comprise information on $d = 486$ SNPs belonging to $K = 33$ genes obtained from a total $n = 632$ subjects (179 cognitively normal (CN), 144 Alzheimers disease (AD), 309 late mild cognitive impairment (LMCI) stage). The genes for which we have information along with the number of SNPs included for each gene are depicted in Figure 1 of the supplementary material.

We include all 486 SNPs and simulate imaging data from $c = 12$ ROIs, with Study I having $n = 632$ subjects, and Study II having $n = 250$ (83 CN, 83 AD, 84 LMCI) subjects. Study II differs from Study I in that we move to a high-dimensional setting by reducing the value of n so that $n < d$. In each case we set the true values as $\lambda_1^2 = \lambda_2^2 = \sigma^2 = 2$, and set the true values for \mathbf{W} by first simulating $\tau_k^2 \mid \lambda_1^2 \stackrel{ind}{\sim} \text{Gamma}\left(\frac{m_k c + 1}{2}, \frac{\lambda_1^2}{2}\right)$, $k = 1, \dots, K$, and $\omega_i^2 \mid \lambda_2^2 \stackrel{ind}{\sim} \text{Gamma}\left(\frac{c + 1}{2}, \frac{\lambda_2^2}{2}\right)$, $i = 1, \dots, d$, and then simulating the regression coefficients from (6), and finally, the true values for \mathbf{W} are obtained by setting the entries of all but 50 rows of \mathbf{W} to zero. This adds additional sparsity to the SNP effects and makes the simulation setup more realistic. We note that the simulation of $\boldsymbol{\tau}^2$ and $\boldsymbol{\omega}^2$ from Gamma distributions is not based on our assumed model and the additional sparsity added after simulation from (6) does not correspond to the prior from our model, so that we are not assuming that the model is correctly specified. The non-zero rows correspond to 5 genes containing exactly 14, 10, 6, 4, and 1 SNP(s) respectively (for a total of 35 SNPs), along with an additional 15 rows corresponding to additional SNPs. The imaging data are simulated from (2) and we note that the model assumption (2) is common to both of the approaches being compared, so neither has an advantage.

To further investigate the robustness of our approach relative to the bootstrap in settings where the model assumptions do not match the model from which the data have been generated we conduct two additional simulation studies, labelled Study III and Study IV, which have the same settings as Study I and Study II, respectively, with the exception that the regression errors are drawn from a heavy-tailed multivariate t_4 distribution.

For each of 100 simulation replicates we compute the bootstrap 95% confidence interval based on the estimator (1) and the posterior distribution from our Bayesian model using the Gibbs sampling algorithm. In total each simulation study involves $d \times c = 5,832$ regression

Table 1: Simulation studies - interval estimation. The coverage probability of each approximate 95% credible/confidence interval is estimated based on 100 simulation replicates and then averaged (MCP) overall and also separately over the parameters that correspond to active SNPs.

Study I		
Method	MCP (overall)	MCP ($w_{ij} \neq 0$)
Bayesian Model	0.95	0.83
Nonparametric Bootstrap	0.85	0.45
Study II		
Method	MCP (overall)	MCP ($w_{ij} \neq 0$)
Bayesian Model	0.94	0.72
Nonparametric Bootstrap	0.85	0.42
Study III		
Method	MCP (overall)	MCP ($w_{ij} \neq 0$)
Bayesian Model	0.97	0.77
Nonparametric Bootstrap	0.86	0.49
Study IV		
Method	MCP (overall)	MCP ($w_{ij} \neq 0$)
Bayesian Model	0.95	0.73
Nonparametric Bootstrap	0.84	0.41

parameters and we use the 100 simulation replicates to estimate the coverage probability of the 95% equal-tail confidence/credible intervals for each parameter. The results are presented in Table 1.

In Study I we find that the mean (over all 5,832 parameters) coverage probability is 95% for intervals constructed based on our approach, while that for the nonparametric bootstrap applied to the estimator of Wang et al. (2012) is 85%, below the nominal level. Considering only those 600 parameters with non-zero effects the mean coverage probability for our approach drops to 83%, while that for the nonparametric bootstrap drops to an unreasonable 45%. In Study II ($n < d$) we find that the mean (over all 5,832 parameters) coverage probability is 94% for our approach while that obtained for intervals constructed using the nonparametric bootstrap is 85%. Considering only those parameters with non-zero true values the mean coverage probabilities associated with both approaches drops as in Study I, to 72% for our approach and to 42% for the nonparametric bootstrap. The results for Studies III and IV generally indicate the same patterns as those seen in Studies I and II, demonstrating that our comparisons exhibit some robustness to model misspecification.

We find that the Bayesian approach is clearly outperforming the estimator of Wang et al. (2012) combined with the nonparametric bootstrap in all cases. In all four studies the mean coverage probability drops when considering only active SNPs, but in this case the values obtained from the nonparametric bootstrap are unreasonably low while those obtained from our approach are still somewhat reasonable, in particular since these coverage probabilities pertain to active SNPs, and therefore, under-coverage will not lead to a false rejection of the null hypothesis.

Table 2: Imaging phenotypes defined as volumetric or cortical thickness measures of $28 \times 2 = 56$ regions of interest (ROIs) from automated Freesurfer parcellations. Each of the phenotypes in the table corresponds to two phenotypes in the data: one for the left hemisphere and the other for the right hemisphere.

ID	Measurement	Region of interest
AmygVol	Volume	Amygdala
CerebCtx	Volume	Cerebral cortex
CerebWM	Volume	Cerebral white matter
HippVol	Volume	Hippocampus
InfLatVent	Volume	Inferior lateral ventricle
LatVent	Volume	Lateral ventricle
EntCtx	Thickness	Entorhinal cortex
Fusiform	Thickness	Fusiform gyrus
InfParietal	Thickness	Inferior parietal gyrus
InfTemporal	Thickness	Inferior temporal gyrus
MidTemporal	Thickness	Middle temporal gyrus
Parahipp	Thickness	Parahippocampal gyrus
PostCing	Thickness	Posterior cingulate
Postcentral	Thickness	Postcentral gyrus
Precentral	Thickness	Precentral gyurs
Precuneus	Thickness	Precuneus
SupFrontal	Thickness	Superior frontal gyrus
SupParietal	Thickness	Superior parietal gyrus
SupTemporal	Thickness	Superior temporal gyrus
Supramarg	Thickness	Supramarginal gyrus
TemporalPole	Thickness	Temporal pole
MeanCing	Mean thickness	Caudal anterior cingulate, isthmus cingulate, posterior cingulate, rostral anterior cingulate
MeanFront	Mean thickness	Caudal midfrontal, rostral midfrontal, superior frontal, lateral orbitofrontal, and medial orbitofrontal gyri, frontal pole
MeanLatTemp	Mean thickness	Inferior temporal, middle temporal, and superior temporal gyri
MeanMedTemp	Mean thickness	Fusiform, parahippocampal, and lingual gyri, temporal pole and transverse temporal pole
MeanPar	Mean thickness	Inferior and superior parietal gyri, supramarginal gyrus, and precuneus
MeanSensMotor	Mean thickness	Precentral and postcentral gyri
MeanTemp	Mean thickness	Inferior temporal, middle temporal, superior temporal, fusiform, parahippocampal, lingual gyri, temporal pole, transverse temporal pole

5 Application to ADNI Data

We illustrate our methodology by applying it to a dataset obtained from the Alzheimer’s Disease Neuroimaging Initiative (ADNI-1) database. This dataset includes both genetic and structural MRI data and is similar to a dataset analyzed by Wang et al. (2012); however, we use a larger number of regions of interest in our analysis leading to 56 imaging phenotypes rather than the 12 imaging phenotypes analyzed by Wang et al. (2012). The imaging phenotypes used in our analysis are listed in Table 2.

Registered ADNI investigators may obtain the preprocessed data used in this analysis by contacting the corresponding author. These data can be used in conjunction with our R package ‘bgsmttr’ implementing our methodology to reproduce the results presented here.

The data are available for $n = 632$ subjects (179 CN, 144 AD, 309 LMCI), and among all possible SNPs we include only those SNPs belonging to the top 40 Alzheimer’s Disease (AD) candidate genes listed on the AlzGene database as of June 10, 2010. The data presented here are queried from the most recent genome build as of December 2014, from the ADNI-1 data.

After quality control and imputation steps, the genetic data used for this study includes 486 SNPs from 33 genes and these genes along with the distribution of the number of SNPs within each gene is depicted in Figure 1 of the supplementary material. The freely

available software package PLINK (Purcell et.al., 2007) was used for genomic quality control. Thresholds used for SNP and subject exclusion were the same as in Wang et. al. (2012), with the following exceptions. For SNPs, we required a more conservative genotyping call rate of at least 95% (Ge et al. 2012).

For subjects, we required at least one baseline and one follow-up MRI scan and excluded multivariate outliers. Sporadically missing genotypes at SNPs in the HapMap3 reference panel (Gibbs et. al., 2003) were imputed into the data using IMPUTE2 (Howie et. al., 2009). Further details of the quality control and imputation procedure can be found in Szefer (2014). The MRI data from the ADNI-1 database are preprocessed using the FreeSurfer V4 software which conducts automated parcellation to define volumetric and cortical thickness values from the $c = 56$ brain regions of interest that are detailed in Table 2. Each of the response variables are adjusted for age, gender, education, handedness, and baseline total intracranial volume (ICV) based on regression weights from healthy controls and are then scaled and centered to have zero-sample-mean and unit-sample-variance.

We fit our model, which for the current dataset has 27,216 regression parameters, by running a total of 49 Gibbs sampling chains in parallel on a computing cluster with each chain corresponding to a different value of $(\lambda_1^2, \lambda_2^2)$, and the WAIC is applied to select which of the 49 chains to use for posterior inference. The Wang et al. (2012) estimator is also computed with tuning parameters γ_1 and γ_2 in (1) set based on $\gamma_1 = 2\sigma\lambda_1$ and $\gamma_2 = 2\sigma\lambda_2$, where the values of λ_1 and λ_2 chosen using WAIC and the posterior mean for σ from the Gibbs sampler are used.

To select potentially important SNPs we evaluate the 95% equal-tail credible interval for each regression coefficient and select those SNPs where at least one of the associated credible intervals excludes 0. In total there are 45 SNPs and 152 regression coefficients for which this occurs. Table 1 in the supplementary material lists each of the 152 SNP-ROI associations along with the corresponding point and interval estimates.

The 45 selected SNPs and the corresponding phenotypes at which we see a potential association based on the 95% credible interval are listed in Table 3. Three SNPs, rs4311 from the ACE gene, rs405509 from the APOE gene, and rs10787010 from the SORCS1 gene stand out as being potentially associated with the largest number of ROIs. The 95% credible intervals for the coefficients relating rs4311 to each of the $c = 56$ imaging measures are depicted in Figure 3, while similar figures for rs405509 and rs10787010 are presented in Figure 2 and Figure 3 of the supplementary material.

In the original methodology of Wang et al. (2012) the authors suggest ranking and selecting SNPs by constructing a SNP weight based on the point estimate $\hat{\mathbf{W}}$ and a sum of the absolute values of the estimated coefficients of each single SNP over all of the tasks. Doing so, the top 45 highest ranked SNPs contains 21 of the SNPs chosen using our approach and these 21 SNPs are highlighted in Table 3. The number 1 ranked (highest priority) SNP using this approach is SNP rs3026841 from gene ECE1. In Figure 4 we display the corresponding point estimates along with the 95% credible intervals (obtained via our Gibbs sampler) relating this SNP to each of the $c = 56$ imaging measures. **We note that all 56 of the corresponding 95% credible intervals include the value 0.** This result demonstrates

Table 3: The 45 SNPs selected from the Bayesian model along with corresponding phenotypes where (L), (R), (L,R) denote that the phenotypes are on the left, right, and both hemispheres respectively. SNPs also ranked among the top 45 using the Wang et al. (2012) estimate are listed in bold.

SNP	Gene	Phenotype ID (Hemisphere)
rs4305	ACE	LatVent (R)
rs4311	ACE	InfParietal (L,R), MeanPar (L,R), Precuneus (L,R), SupParietal (L), SupTemporal (L), CerebCtx (R), MeanFront (R), MeanSensMotor (R), MeanTemp (R), Postcentral (R), PostCing (R), Precentral (R), SupFrontal (R), SupParietal (R)
rs405509	APOE	AmygVol (L), CerebWM (L), Fusiform (L), HippVol (L), InfParietal (L,R), SupFrontal (L,R), Supramarg (L,R), InfTemporal (L), MeanFront (L,R), MeanLatTemp (L,R), MeanMedTemp (L,R), MeanPar (L,R), MeanSensMotor (L,R), MeanTemp (L,R), MidTemporal (L,R), Postcentral (L,R), Precuneus (L,R) SupTemporal (L,R), Precentral (R), SupParietal (R)
rs11191692	CALHM1	EntCtx (L)
rs3811450	CHRNA2	Precuneus (R)
rs9314349	CLU	Parahipp (L)
rs2025935	CR1	CerebWM (R), Fusiform (R), InfLatVent (R)
rs11141918	DAPK1	CerebCtx (R)
rs1473180	DAPK1	CerebCtx (L,R), EntCtx (L), Fusiform (L), MeanMedTemp (L), MeanTemp (L), PostCing (L)
rs17399090	DAPK1	MeanCing (R), PostCing (R)
rs3095747	DAPK1	InfLatVent (R)
rs3118846	DAPK1	InfParietal (R)
rs3124237	DAPK1	PostCing (R), Precuneus (R), SupFrontal (R)
rs4878117	DAPK1	MeanSensMotor (R), Postcentral (R)
rs212539	ECE1	PostCing (R)
rs6584307	ENTPD7	Parahipp (L)
rs11601726	GAB2	CerebWM (L), LatVent (L)
rs16924159	IL33	MeanCing (L), PostCing (L), CerebWM (R)
rs928413	IL33	InfLatVent (R)
rs1433099	LDLR	CerebCtx.adj (L), Precuneus (L,R)
rs2569537	LDLR	CerebWM (L,R)
rs12209631	NEDD9	CerebCtx (L), HippVol (L,R)
rs1475345	NEDD9	Parahipp (L)
rs17496723	NEDD9	Supramarg (L)
rs2327389	NEDD9	AmygVol (L)
rs744970	NEDD9	MeanFront (L), SupFrontal (L)
rs7938033	PICALM	EntCtx (R), HippVol (R)
rs2756271	PRNP	EntCtx (L), HippVol (L,R), InfTemporal (L), Parahipp (L)
rs6107516	PRNP	MidTemporal (L,R)
rs1023024	SORCS1	MeanSensMotor (L), Precentral (L)
rs10787010	SORCS1	AmygVol (L), EntCtx (L,R), Fusiform (L), HippVol (L,R), InfLatVent (L), InfTemporal (L), MeanFront (L), MeanMedTemp (L,R), MeanTemp (L), Precentral (L), TemporalPole (R)
rs10787011	SORCS1	EntCtx (L,R), HippVol(R)
rs12248379	SORCS1	PostCing (R)
rs1269918	SORCS1	CerebCtx (L), CerebWM (L), InfLatVent (L)
rs1556758	SORCS1	SupParietal (L)
rs2149196	SORCS1	MeanSensMotor (L), Postcentral (L,R)
rs2418811	SORCS1	CerebWM (L,R), InfLatVent.adj (L)
rs10502262	SORL1	MeanCing (L), InfTemporal (R), Supramarg (R)
rs1699102	SORL1	MeanMedTemp (R), MeanTemp (R)
rs1699105	SORL1	MeanCing (L), Precuneus (L)
rs4935774	SORL1	CerebWM (L,R)
rs666004	SORL1	InfTemporal (L)
rs1568400	THRA	Precentral (L), TemporalPole (R)
rs3744805	THRA	MeanSensMotor (R), Postcentral (R), Precentral (R)
rs7219773	TNK1	MeanSensMotor (L), Precentral (L), Postcentral (R)

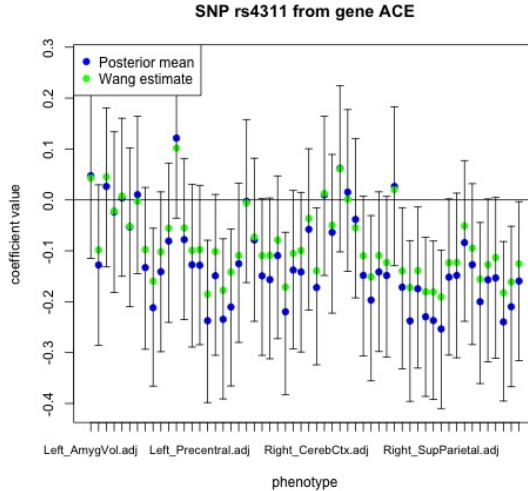


Figure 3: The 95% equal-tail credible intervals relating the SNP rs4311 from ACE to each of the $c = 56$ imaging phenotypes, represented on the x-axis in the same order as they are listed in the rows of Table 2, first for the left hemisphere followed by the right.

clearly the importance of accounting for posterior uncertainty beyond the point estimate and illustrates the potential problems that may arise when estimation uncertainty is ignored. It thus serves to illustrate the practical value of our proposed methodology.

6 Conclusion

We have proposed a framework for the analysis of data arising in studies of imaging genomics that extends a previously developed regularization approach in order to allow for the quantification of estimation (posterior) uncertainty in multi-task regression with a $G_{2,1}$ - norm penalty. The value added of our approach has been demonstrated using both simulation studies as well as the analysis of a real dataset from the ADNI database. We have compared our approach to the nonparametric bootstrap applied to (1) and have demonstrated that our methodology clearly outperforms the latter in terms of mean coverage probability, for the settings considered. We note that our implementation of the bootstrap estimates the tuning parameters from the dataset using cross-validation and subsequently these parameters are fixed across all bootstrap replicates. To keep the computational burden down, it is routine to fix tuning parameters when bootstrapping; however, fixing these parameters does ignore the uncertainty associated with the estimated tuning parameters and this may be contributing to the bias towards below-nominal coverage in the bootstrap intervals. Re-estimating the tuning parameters for each bootstrap replicate is computationally infeasible without massively parallel computers.

It should be noted that we have not addressed statistical adjustments for multiplicity; however, our contribution is a step forward in moving from point estimation to posterior

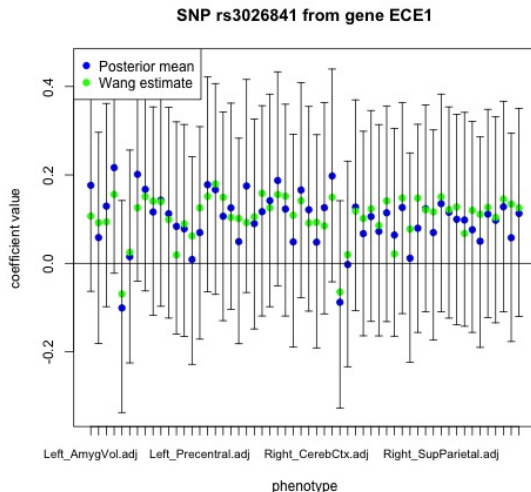


Figure 4: The 95% equal-tail credible intervals relating the SNP rs3026841 from ECE1 to each of the $c = 56$ imaging phenotypes represented on the x-axis in the same order as they are listed in the rows of Table 2, first for the left hemisphere followed by the right.

distributions for this regression model. Bayesian false discovery rate procedures (Morris et al., 2008) can be used to adjust for multiplicity in the selection of SNPs based on the output of the Gibbs sampler and this will be considered in future work.

We are currently investigating an extension of the model that allows for a more flexible covariance structure in the specification (2), and alternative shrinkage prior formulations such as the horseshoe prior (Carvalho et al., 2010) that could potentially be further developed for the type of bi-level penalization we have considered here. An alternative approach that is potentially of interest in allowing for increased scalability of the proposed model is the use of a low-rank approximation to the regression coefficient matrix \mathbf{W} as considered in Marttinen et al. (2014), though this would require an appropriate choice for the rank of the regression model. The sparsity structure we propose in this article could then be incorporated into such an approximation as an extension to the current approach. In addition, extending our model to accommodate potential hidden confounding factors through a joint modelling approach as considered in Fusi et al. (2012), and the incorporation of terms allowing for gene-gene interactions are interesting avenues for future work.

Acknowledgements

Research is supported by funding from the Natural Sciences and Engineering Research Council of Canada. F.S. Nathoo holds a Tier II Canada Research Chair in Biostatistics for Spatial and High-Dimensional Data. Research was enabled in part by support provided by West-Grid (www.westgrid.ca) and Compute Canada (www.computecanada.ca) with assistance

provided by HPC specialist Dr. Belaid Moa. Data collection and sharing for this project was funded by the Alzheimer’s Disease Neuroimaging Initiative (ADNI) (National Institutes of Health Grant U01 AG024904) and DOD ADNI (Department of Defense award number W81XWH-12-2-0012). The authors thank Dr. Faisal Beg and Donghuan Lu for assistance with preprocessing of the ADNI MRI data. This work was based on Keelin Greenlaw’s MSc thesis supervised by F.S. Nathoo and M. Lesperance.

References

- [1] Kyoung-hwa Bae and Bani K Mallick. Gene selection using a two-level hierarchical Bayesian model. *Bioinformatics*, 20(18):3423–3430, 2004.
- [2] Carlos M Carvalho, Nicholas G Polson, and James G Scott. The horseshoe estimator for sparse signals. *Biometrika*, pp. 465–480, 2010.
- [3] A Evgeniou and Massimiliano Pontil. Multi-task feature learning. *Advances in neural information processing systems*, 19:41, 2007.
- [4] Nicolás Fusi, Oliver Stegle, and Neil D Lawrence. Joint modelling of confounding factors and prominent genetic regulators provides increased accuracy in genetical genomics studies. *PLoS Comput Biol*, 8(1):e1002330, 2012.
- [5] Tian Ge, Jianfeng Feng, Derrek P Hibar, Paul M Thompson, and Thomas E Nichols. Increasing power for voxel-wise genome-wide association studies: the random field theory, least square kernel machines and fast permutation procedures. *Neuroimage*, 63(2):858–873, 2012.
- [6] Tian Ge, Gunter Schumann, and Jianfeng Feng. Imaging genetics — towards discovery neuroscience. *Quantitative Biology*, 1(4):227–245, 2013.
- [7] Andrew Gelman, Jessica Hwang, and Aki Vehtari. Understanding predictive information criteria for Bayesian models. *Statistics and Computing*, 24(6):997–1016, 2014.
- [8] Derrek P Hibar, Jason L Stein, Omid Kohannim, Neda Jahanshad, Andrew J Saykin, Li Shen, Sungeun Kim, Nathan Pankratz, Tatiana Foroud, Matthew J Huentelman, et al. Voxelwise gene-wide association study (vgenewas): multivariate gene-based association testing in 731 elderly subjects. *Neuroimage*, 56(4):1875–1891, 2011.
- [9] Bryan N Howie, Peter Donnelly, and Jonathan Marchini. A flexible and accurate genotype imputation method for the next generation of genome-wide association studies. *PLoS Genet*, 5(6):e1000529, 2009.
- [10] Samuel Kotz, Tomasz Kozubowski, and Krzysztof Podgorski. *The Laplace distribution and generalizations: a revisit with applications to communications, economics, engineering, and finance*. Springer Science & Business Media, 2012.

- [11] Minjung Kyung, Jeff Gill, Malay Ghosh, George Casella, et al. Penalized regression, standard errors, and Bayesian lassos. *Bayesian Analysis*, 5(2):369–411, 2010.
- [12] Pekka Marttinen, Matti Pirinen, Antti-Pekka Sarin, Jussi Gillberg, Johannes Kettunen, Ida Surakka, Antti J Kangas, Pasi Soininen, Paul O'Reilly, Marika Kaakinen, et al. Assessing multivariate gene-metabolome associations with rare variants using bayesian reduced rank regression. *Bioinformatics*, p. btu140, 2014.
- [13] Jeffrey S Morris, Philip J Brown, Richard C Herrick, Keith A Baggerly, and Kevin R Coombes. Bayesian analysis of mass spectrometry proteomic data using wavelet-based functional mixed models. *Biometrics*, 64(2):479–489, 2008.
- [14] Farouk S Nathoo, Keelin Greenlaw, and Mary Lesperance. Regularization parameter selection for a Bayesian group sparse multi-task regression model with application to imaging genomics. In *Pattern Recognition in Neuroimaging (PRNI), 2016 International Workshop on*, pp. 1–4. IEEE, 2016.
- [15] Trevor Park and George Casella. The Bayesian lasso. *Journal of the American Statistical Association*, 103(482):681–686, 2008.
- [16] Shaun Purcell, Benjamin Neale, Kathe Todd-Brown, Lori Thomas, Manuel AR Ferreira, David Bender, Julian Maller, Pamela Sklar, Paul IW De Bakker, Mark J Daly, et al. Plink: a tool set for whole-genome association and population-based linkage analyses. *The American Journal of Human Genetics*, 81(3):559–575, 2007.
- [17] Sylvia Richardson, Leonardo Bottolo, and Jeffrey S Rosenthal. Bayesian models for sparse regression analysis of high dimensional data. *Bayesian Statistics*, 9:539–569, 2010.
- [18] Veronika Rockova, Emmanuel Lesaffre, et al. Incorporating grouping information in Bayesian variable selection with applications in genomics. *Bayesian Analysis*, 9(1):221–258, 2014.
- [19] Jason L Stein, Xue Hua, Suh Lee, April J Ho, Alex D Leow, Arthur W Toga, Andrew J Saykin, Li Shen, Tatiana Foroud, Nathan Pankratz, et al. Voxelwise genome-wide association study (vgwas). *neuroimage*, 53(3):1160–1174, 2010.
- [20] Francesco C Stingo, Yian A Chen, Mahlet G Tadesse, and Marina Vannucci. Incorporating biological information into linear models: A Bayesian approach to the selection of pathways and genes. *The annals of applied statistics*, 5(3), 2011.
- [21] Francesco C Stingo, Michele Guindani, Marina Vannucci, and Vince D Calhoun. An integrative Bayesian modeling approach to imaging genetics. *Journal of the American Statistical Association*, 108(503):876–891, 2013.
- [22] Elena Kaarina Szefer. Joint analysis of imaging and genomic data to identify associations related to cognitive impairment. MSc Thesis, Simon Fraser University. 2014.

- [23] Maria Vounou, Thomas E Nichols, Giovanni Montana, and Alzheimer’s Disease Neuroimaging Initiative. Discovering genetic associations with high-dimensional neuroimaging phenotypes: a sparse reduced-rank regression approach. *Neuroimage*, 53(3):1147–1159, 2010.
- [24] Hua Wang, Feiping Nie, Heng Huang, Sungeun Kim, Kwangsik Nho, Shannon L Risacher, Andrew J Saykin, Li Shen, et al. Identifying quantitative trait loci via group-sparse multitask regression and feature selection: an imaging genetics study of the ADNI cohort. *Bioinformatics*, 28(2):229–237, 2012.
- [25] Sumio Watanabe. Asymptotic equivalence of Bayes cross validation and widely applicable information criterion in singular learning theory. *The Journal of Machine Learning Research*, 11:3571–3594, 2010.
- [26] Xiaoquan Wen. Bayesian model selection in complex linear systems, as illustrated in genetic association studies. *Biometrics*, 70(1):73–83, 2014.
- [27] Keith J Worsley, Sean Marrett, Peter Neelin, Alain C Vandal, Karl J Friston, Alan C Evans, et al. A unified statistical approach for determining significant signals in images of cerebral activation. *Human brain mapping*, 4(1):58–73, 1996.
- [28] KJ Worsley. Non-stationary FWHM and its effect on statistical inference of fMRI data. *NeuroImage*, 15(346):779–790, 2002.
- [29] Ming Yuan and Yi Lin. Model selection and estimation in regression with grouped variables. *Journal of the Royal Statistical Society: Series B (Statistical Methodology)*, 68(1):49–67, 2006.
- [30] Hongtu Zhu, Zakaria Khondker, Zhaohua Lu, and Joseph G Ibrahim. Bayesian generalized low rank regression models for neuroimaging phenotypes and genetic markers. *Journal of the American Statistical Association*, 109(507):977–990, 2014.

Supplemental Materials: 'A Bayesian Group Sparse Multi-Task Regression Model for Imaging Genetics'

1 Derivations for the Gibbs Sampling Algorithm

Here we derive the full conditional distributions required for Gibbs sampling. In what follows we make use of the vectorisation of a matrix, \mathbf{A} , a linear transformation of \mathbf{A} to a column vector in which the columns of \mathbf{A} are stacked one under the other to form a single column. Eg. If \mathbf{A} is a $d \times c$ matrix, then $\text{vec}(\mathbf{A}^T) = [A_{1,1}, \dots, A_{1,c}, A_{2,1}, \dots, A_{2,c}, \dots, A_{d,1}, \dots, A_{d,c}]^T$. We will further make use of the result $\text{vec}(\mathbf{A}\mathbf{B}) = (\mathbf{B}^T \otimes \mathbf{I}_k)\text{vec}(\mathbf{A})$, where k is the number of rows in \mathbf{A} and \otimes denotes the Kronecker product.

Assuming the scale mixture representation of the product multivariate Laplace distribution presented in Proposition 2, the joint posterior distribution can be expressed up to a normalizing constant as

$$\begin{aligned}
 p(\mathbf{W}, \tau_1^2, \dots, \tau_K^2, \omega_1^2, \dots, \omega_d^2, \sigma^2 | \mathbf{Y}) &\propto p(\mathbf{Y} | \mathbf{W}, \sigma^2) p(\mathbf{W} | \sigma^2, \boldsymbol{\tau}^2, \boldsymbol{\omega}) p(\boldsymbol{\tau}^2, \boldsymbol{\omega}^2 | \lambda_1^2, \lambda_2^2) p(\sigma^2 | a_\sigma, b_\sigma) \\
 &\propto |\sigma^2 \mathbf{I}_c|^{-\frac{n}{2}} \exp \left\{ -\frac{1}{2\sigma^2} \sum_{\ell=1}^n (\mathbf{y}_\ell - \mathbf{W}^T \mathbf{x}_\ell)^T (\mathbf{y}_\ell - \mathbf{W}^T \mathbf{x}_\ell) \right\} \\
 &\times \prod_{k=1}^K \left[\prod_{i \in \pi_k} \left[\left(\sigma^2 \left(\frac{1}{\tau_k^2} + \frac{1}{\omega_i^2} \right)^{-1} \right)^{-\frac{c}{2}} \right] \exp \left\{ -\sum_{i \in \pi_k} \left(\frac{\sum_{j=1}^c w_{ij}^2}{2\sigma^2 \left(\frac{1}{\tau_k^2} + \frac{1}{\omega_i^2} \right)^{-1}} \right) \right\} \right] \\
 &\times \prod_{k=1}^K \left(\frac{\lambda_1^2}{2} \right)^{\left(\frac{m_k c + 1}{2} \right)} (\tau_k^2)^{\left(\frac{m_k c + 1}{2} \right) - 1} \exp \left\{ -\left(\frac{\lambda_1^2}{2} \right) \tau_k^2 \right\} \\
 &\times \left[\prod_{i \in \pi_k} \left(\frac{\lambda_2^2}{2} \right)^{\left(\frac{c+1}{2} \right)} (\omega_i^2)^{\left(\frac{c+1}{2} \right) - 1} \exp \left\{ -\left(\frac{\lambda_2^2}{2} \right) \omega_i^2 \right\} (\tau_k^2 + \omega_i^2)^{-\frac{c}{2}} \right] \\
 &\times \frac{b_\sigma^{a_\sigma}}{\Gamma(a_\sigma)} (\sigma^2)^{-a_\sigma - 1} \exp \left\{ -\frac{b_\sigma}{\sigma^2} \right\}.
 \end{aligned}$$

Full conditional distribution of $\mathbf{W}^{(k)}$

$$\begin{aligned}
 p(\mathbf{W}^{(k)} | \mathbf{Y}, \mathbf{W}^{(-k)}, \boldsymbol{\tau}^2, \boldsymbol{\omega}^2, \sigma^2, \lambda_1^2, \lambda_2^2) &\propto \\
 &\exp \left\{ \frac{-1}{2\sigma^2} \sum_{\ell=1}^n (\mathbf{y}_\ell - \mathbf{W}^T \mathbf{x}_\ell)^T (\mathbf{y}_\ell - \mathbf{W}^T \mathbf{x}_\ell) \right\} \exp \left\{ -\sum_{i \in \pi_k} \left(\frac{\sum_{j=1}^c w_{ij}^2}{2\sigma^2 \left(\frac{1}{\tau_k^2} + \frac{1}{\omega_i^2} \right)^{-1}} \right) \right\}. \quad (\text{S1})
 \end{aligned}$$

Split \mathbf{W} into $\mathbf{W}^{(k)}$ and $\mathbf{W}^{(-k)}$ and rewrite the first exponent of (S1) as

$$\exp \left\{ \frac{-1}{2\sigma^2} \sum_{\ell=1}^n (\mathbf{y}_\ell - \mathbf{W}^{(k)T} \mathbf{x}_\ell^{(k)} - \mathbf{W}^{(-k)T} \mathbf{x}_\ell^{(-k)})^T (\mathbf{y}_\ell - \mathbf{W}^{(k)T} \mathbf{x}_\ell^{(k)} - \mathbf{W}^{(-k)T} \mathbf{x}_\ell^{(-k)}) \right\}. \quad (\text{S2})$$

We vectorise the terms that include either $\mathbf{W}^{(k)}$ or $\mathbf{W}^{(-k)}$ and simplify based on:

- 1) $\text{vec}(\mathbf{W}^{(k)T} \mathbf{x}_\ell^{(k)}) = (\mathbf{x}_\ell^{(k)T} \otimes I_c) \text{vec}(\mathbf{W}^{(k)T})$
- 2) $\text{vec}(\mathbf{W}^{(-k)T} \mathbf{x}_\ell^{(-k)}) = (\mathbf{x}_\ell^{(-k)T} \otimes I_c) \text{vec}(\mathbf{W}^{(-k)T})$.

These results give an equivalent expression for (S2)

$$\exp \left\{ \frac{-1}{2\sigma^2} \sum_{\ell=1}^n \left(\mathbf{y}_\ell - (\mathbf{x}_\ell^{(k)T} \otimes I_c) \text{vec}(\mathbf{W}^{(k)T}) - (\mathbf{x}_\ell^{(-k)T} \otimes I_c) \text{vec}(\mathbf{W}^{(-k)T}) \right)^T \right. \\ \left. \left(\mathbf{y}_\ell - (\mathbf{x}_\ell^{(k)T} \otimes I_c) \text{vec}(\mathbf{W}^{(k)T}) - (\mathbf{x}_\ell^{(-k)T} \otimes I_c) \text{vec}(\mathbf{W}^{(-k)T}) \right) \right\}$$

which can be expressed as

$$\exp \left\{ \frac{-1}{2\sigma^2} \sum_{\ell=1}^n \left(\mathbf{y}_\ell^T - \text{vec}(\mathbf{W}^{(k)T})^T (\mathbf{x}_\ell^{(k)T} \otimes I_c)^T - \text{vec}(\mathbf{W}^{(-k)T})^T (\mathbf{x}_\ell^{(-k)T} \otimes I_c)^T \right) \right. \\ \left. \left(\mathbf{y}_\ell - (\mathbf{x}_\ell^{(k)T} \otimes I_c) \text{vec}(\mathbf{W}^{(k)T}) - (\mathbf{x}_\ell^{(-k)T} \otimes I_c) \text{vec}(\mathbf{W}^{(-k)T}) \right) \right\}$$

Using $(A \otimes B)^T = (A^T \otimes B^T)$ the above is simplified to

$$\exp \left\{ \frac{-1}{2\sigma^2} \sum_{\ell=1}^n \left(\mathbf{y}_\ell^T - \text{vec}(\mathbf{W}^{(k)T})^T (\mathbf{x}_\ell^{(k)} \otimes I_c) - \text{vec}(\mathbf{W}^{(-k)T})^T (\mathbf{x}_\ell^{(-k)} \otimes I_c) \right) \right. \\ \left. \left(\mathbf{y}_\ell - (\mathbf{x}_\ell^{(k)T} \otimes I_c) \text{vec}(\mathbf{W}^{(k)T}) - (\mathbf{x}_\ell^{(-k)T} \otimes I_c) \text{vec}(\mathbf{W}^{(-k)T}) \right) \right\}.$$

It is now possible to expand the expression. Only those terms that include $\mathbf{W}^{(k)}$ are kept, as the other terms are considered to be constants that can be factored out to become part of the normalising constant. We have

$$\exp \left\{ \frac{-1}{2\sigma^2} \sum_{\ell=1}^n \left(-\mathbf{y}_\ell^T (\mathbf{x}_\ell^{(k)T} \otimes I_c) \text{vec}(\mathbf{W}^{(k)T}) - \text{vec}(\mathbf{W}^{(k)T})^T (\mathbf{x}_\ell^{(k)} \otimes I_c) \mathbf{y}_\ell \right. \right. \\ \left. \left. + \text{vec}(\mathbf{W}^{(k)T})^T (\mathbf{x}_\ell^{(k)} \otimes I_c) (\mathbf{x}_\ell^{(k)T} \otimes I_c) \text{vec}(\mathbf{W}^{(k)T}) \right. \right. \\ \left. \left. + \text{vec}(\mathbf{W}^{(k)T})^T (\mathbf{x}_\ell^{(k)} \otimes I_c) (\mathbf{x}_\ell^{(-k)T} \otimes I_c) \text{vec}(\mathbf{W}^{(-k)T}) \right. \right. \\ \left. \left. + \text{vec}(\mathbf{W}^{(-k)T})^T (\mathbf{x}_\ell^{(-k)} \otimes I_c) (\mathbf{x}_\ell^{(k)T} \otimes I_c) \text{vec}(\mathbf{W}^{(k)T}) \right) \right\}$$

which can be expressed as

$$\exp \left\{ \frac{-1}{2\sigma^2} \left[\text{vec}(\mathbf{W}^{(k)T})^T \sum_{\ell=1}^n (\mathbf{x}_\ell^{(k)} \otimes I_c) (\mathbf{x}_\ell^{(k)T} \otimes I_c) \text{vec}(\mathbf{W}^{(k)T}) \right. \right. \\ \left. \left. + 2 \text{vec}(\mathbf{W}^{(k)T})^T \sum_{\ell=1}^n (\mathbf{x}_\ell^{(k)} \otimes I_c) (\mathbf{x}_\ell^{(-k)T} \otimes I_c) \text{vec}(\mathbf{W}^{(-k)T}) - 2 \text{vec}(\mathbf{W}^{(k)T})^T \sum_{\ell=1}^n (\mathbf{x}_\ell^{(k)} \otimes I_c) \mathbf{y}_\ell \right] \right\}.$$

Next, consider the second exponent in (S1),

$$\exp \left\{ \frac{-1}{2\sigma^2} \sum_{i \in \pi_k} \frac{\sum_{j=1}^c w_{ij}^2}{\left(\frac{1}{\tau_k^2} + \frac{1}{\omega_i^2}\right)^{-1}}, \right\}$$

and define a matrix, \mathbf{H}_k , such that $\mathbf{H}_k = \left[\text{diag} \left\{ \frac{1}{\tau_k^2} + \frac{1}{\omega_i^2} \right\}_{i \in \pi_k} \otimes I_c \right]$.

Notice that,

$$\sum_{i \in \pi_k} \frac{\sum_{j=1}^c w_{ij}^2}{\left(\frac{1}{\tau_k^2} + \frac{1}{\omega_i^2}\right)^{-1}} = \text{vec}(\mathbf{W}^{(k)T})^T \mathbf{H}_k \text{vec}(\mathbf{W}^{(k)T}).$$

We can then rewrite (S1), up to its normalising constant, as,

$$\begin{aligned} p(\mathbf{W}^{(k)} | \mathbf{Y}, \mathbf{W}^{(-k)}, \boldsymbol{\tau}, \boldsymbol{\omega}, \sigma^2, \lambda_1^2, \lambda_2^2) \propto \\ \exp \left\{ \frac{-1}{2\sigma^2} \left[\text{vec}(\mathbf{W}^{(k)T})^T \sum_{\ell=1}^n (\mathbf{x}_\ell^{(k)} \otimes I_c) (\mathbf{x}_\ell^{(k)T} \otimes I_c) \text{vec}(\mathbf{W}^{(k)T}) + \text{vec}(\mathbf{W}^{(k)T})^T \mathbf{H}_k \text{vec}(\mathbf{W}^{(k)T}) \right. \right. \\ \left. \left. + 2 \text{vec}(\mathbf{W}^{(k)T})^T \sum_{\ell=1}^n (\mathbf{x}_\ell^{(k)} \otimes I_c) (\mathbf{x}_\ell^{(-k)T} \otimes I_c) \text{vec}(\mathbf{W}^{(-k)T}) \right. \right. \\ \left. \left. - 2 \text{vec}(\mathbf{W}^{(k)T})^T \sum_{\ell=1}^n (\mathbf{x}_\ell^{(k)} \otimes I_c) \mathbf{y}_\ell \right] \right\}. \quad (\text{S3}) \end{aligned}$$

Expression (S3) is a quadratic form in $\text{vec}(\mathbf{W}^{(k)T})$ in the exponent. Therefore, the full conditional distribution of $\text{vec}(\mathbf{W}^{(k)T})$ is multivariate normal of dimension $m_k c$, with parameters, say, μ_k and Σ_k . After expanding, the exponent of a multivariate normal distribution is of the form,

$$\exp \left\{ -\frac{1}{2} \left[\text{vec}(\mathbf{W}^{(k)T})^T \Sigma_k^{-1} \text{vec}(\mathbf{W}^{(k)T}) - 2 \text{vec}(\mathbf{W}^{(k)T})^T \Sigma_k^{-1} \mu_k + \text{constant} \right] \right\}. \quad (\text{S4})$$

The next steps involve matching (S3) to (S4).

Solving for Σ_k :

Consider the terms of (S3) that are quadratic in $\text{vec}(\mathbf{W}^{(k)T})$. We have

$$\exp \left\{ \frac{-1}{2\sigma^2} \left[\text{vec}(\mathbf{W}^{(k)T})^T \sum_{\ell=1}^n (\mathbf{x}_\ell^{(k)} \otimes I_c) (\mathbf{x}_\ell^{(k)T} \otimes I_c) \text{vec}(\mathbf{W}^{(k)T}) + \text{vec}(\mathbf{W}^{(k)T})^T \mathbf{H}_k \text{vec}(\mathbf{W}^{(k)T}) \right] \right\}.$$

Rearrange to obtain

$$\exp \left\{ -\frac{1}{2} \left[\text{vec}(\mathbf{W}^{(k)T})^T \left(\frac{1}{\sigma^2} \left(\sum_{\ell=1}^n (\mathbf{x}_\ell^{(k)} \otimes I_c) (\mathbf{x}_\ell^{(k)T} \otimes I_c) + \mathbf{H}_k \right) \right) \text{vec}(\mathbf{W}^{(k)T}) \right] \right\}$$

We now observe that

$$\begin{aligned}\boldsymbol{\Sigma}_k^{-1} &= \frac{1}{\sigma^2} \left(\sum_{\ell=1}^n (\mathbf{x}_\ell^{(k)} \otimes I_c)(\mathbf{x}_\ell^{(k)T} \otimes I_c) + \mathbf{H}_k \right), \\ \boldsymbol{\Sigma}_k &= \sigma^2 \left(\sum_{\ell=1}^n (\mathbf{x}_\ell^{(k)} \otimes I_c)(\mathbf{x}_\ell^{(k)T} \otimes I_c) + \mathbf{H}_k \right)^{-1}.\end{aligned}$$

This gives $\boldsymbol{\Sigma}_k = \sigma^2 \mathbf{A}_k^{-1}$,

where $\mathbf{A}_k = \left(\sum_{\ell=1}^n (\mathbf{x}_\ell^{(k)} \otimes I_c)(\mathbf{x}_\ell^{(k)T} \otimes I_c) + \left(\text{diag} \left\{ \frac{1}{\tau_k^2} + \frac{1}{\omega_i^2} \right\}_{i \in \pi_k} \otimes I_c \right) \right)$.

Solving for μ_k :

Consider the term $-\frac{1}{2} \left(-2\text{vec}(\mathbf{W}^{(k)T})^T \boldsymbol{\Sigma}_k^{-1} \mu_k \right)$ within the density of the multivariate normal density. We have the expression,

$$\begin{aligned}& -\frac{1}{2\sigma^2} \left(2\text{vec}(\mathbf{W}^{(k)T})^T \sum_{\ell=1}^n (\mathbf{x}_\ell^{(k)} \otimes I_c)(\mathbf{x}_\ell^{(-k)T} \otimes I_c) \text{vec}(\mathbf{W}^{(-k)T}) - 2\text{vec}(\mathbf{W}^{(k)T})^T \sum_{\ell=1}^n (\mathbf{x}_\ell^{(k)} \otimes I_c) \mathbf{y}_\ell \right) \\ &= \text{vec}(\mathbf{W}^{(k)T})^T \left(\frac{1}{\sigma^2} \left(-\sum_{\ell=1}^n (\mathbf{x}_\ell^{(k)} \otimes I_c)(\mathbf{x}_\ell^{(-k)T} \otimes I_c) \text{vec}(\mathbf{W}^{(-k)T}) + \sum_{\ell=1}^n (\mathbf{x}_\ell^{(k)} \otimes I_c) \mathbf{y}_\ell \right) \right).\end{aligned}$$

Match up the expressions.

$$\boldsymbol{\Sigma}_k^{-1} \mu_k = \frac{1}{\sigma^2} \left(-\sum_{\ell=1}^n (\mathbf{x}_\ell^{(k)} \otimes I_c)(\mathbf{x}_\ell^{(-k)T} \otimes I_c) \text{vec}(\mathbf{W}^{(-k)T}) + \sum_{\ell=1}^n (\mathbf{x}_\ell^{(k)} \otimes I_c) \mathbf{y}_\ell \right).$$

Isolate μ_k to obtain

$$\begin{aligned}\mu_k &= \boldsymbol{\Sigma}_k \left(\frac{1}{\sigma^2} \left(-\sum_{\ell=1}^n (\mathbf{x}_\ell^{(k)} \otimes I_c)(\mathbf{x}_\ell^{(-k)T} \otimes I_c) \text{vec}(\mathbf{W}^{(-k)T}) + \sum_{\ell=1}^n (\mathbf{x}_\ell^{(k)} \otimes I_c) \mathbf{y}_\ell \right) \right) \\ &= \mathbf{A}_k^{-1} \left(-\sum_{\ell=1}^n (\mathbf{x}_\ell^{(k)} \otimes I_c)(\mathbf{x}_\ell^{(-k)T} \otimes I_c) \text{vec}(\mathbf{W}^{(-k)T}) + \sum_{\ell=1}^n (\mathbf{x}_\ell^{(k)} \otimes I_c) \mathbf{y}_\ell \right).\end{aligned}$$

Finally, the full conditional distribution of $\mathbf{W}^{(k)}$ is expressed as

$$\text{vec}(\mathbf{W}^{(k)T}) | \mathbf{Y}, \mathbf{W}^{(-k)}, \boldsymbol{\tau}, \boldsymbol{\omega}, \sigma^2, \lambda_1^2, \lambda_2^2 \sim MVN_{m_k c}(\mu_k, \boldsymbol{\Sigma}_k),$$

where

$$\mu_k = \mathbf{A}_k^{-1} \left(-\sum_{\ell=1}^n (\mathbf{x}_\ell^{(k)} \otimes I_c)(\mathbf{x}_\ell^{(-k)T} \otimes I_c) \text{vec}(\mathbf{W}^{(-k)T}) + \sum_{\ell=1}^n (\mathbf{x}_\ell^{(k)} \otimes I_c) \mathbf{y}_\ell \right),$$

$$\mathbf{A}_k = \left(\sum_{\ell=1}^n (\mathbf{x}_\ell^{(k)} \otimes I_c)(\mathbf{x}_\ell^{(k)T} \otimes I_c) + \left(\text{diag} \left\{ \frac{1}{\tau_k^2} + \frac{1}{\omega_i^2} \right\}_{i \in \pi_k} \otimes I_c \right) \right), \text{ and } \Sigma_k = \sigma^2 \mathbf{A}_k^{-1}.$$

Full conditional distribution of σ^2 :

$$\begin{aligned} p(\sigma^2 | \mathbf{Y}, \mathbf{W}, \boldsymbol{\tau}, \boldsymbol{\omega}, \lambda_1^2, \lambda_2^2) &\propto |\sigma^2 I_c|^{-\frac{n}{2}} \exp \left\{ -\frac{1}{2\sigma^2} \sum_{\ell=1}^n (\mathbf{y}_\ell - \mathbf{W}^T \mathbf{x}_\ell)^T (\mathbf{y}_\ell - \mathbf{W}^T \mathbf{x}_\ell) \right\} \\ &\prod_{k=1}^K \left[(\sigma^2)^{-\frac{m_k c}{2}} \prod_{i \in \pi_k} \left[\left(\frac{1}{\tau_k^2} + \frac{1}{\omega_i^2} \right)^{-1} \right]^{-\frac{c}{2}} \exp \left\{ -\frac{1}{2\sigma^2} \sum_{i \in \pi_k} \frac{\sum_{j=1}^c w_{ij}^2}{\left(\frac{1}{\tau_k^2} + \frac{1}{\omega_i^2} \right)^{-1}} \right\} \right] \cdot (\sigma^2)^{-a_\sigma - 1} \exp \left\{ -\frac{b_\sigma}{\sigma^2} \right\} \\ &= \prod_{k=1}^K \prod_{i \in \pi_k} \left[\left(\frac{1}{\tau_k^2} + \frac{1}{\omega_i^2} \right)^{-1} \right]^{-\frac{c}{2}} (\sigma^2)^{-\frac{cn}{2}} (\sigma^2)^{-\frac{dc}{2}} (\sigma^2)^{-a_\sigma - 1} \\ &\exp \left\{ -\frac{1}{2\sigma^2} \sum_{\ell=1}^n \|\mathbf{y}_\ell - \mathbf{W}^T \mathbf{x}_\ell\|_2^2 - \frac{1}{2\sigma^2} \sum_{i=1}^d \frac{\sum_{j=1}^c w_{ij}^2}{\left(\frac{1}{\tau_{k(i)}^2} + \frac{1}{\omega_i^2} \right)^{-1}} - \frac{b_\sigma}{\sigma^2} \right\}. \end{aligned}$$

Since $\prod_{k=1}^K \prod_{i \in \pi_k} \left[\left(\frac{1}{\tau_k^2} + \frac{1}{\omega_i^2} \right)^{-1} \right]^{-\frac{c}{2}}$ does not depend on σ^2 , it can be factored out of the expression. This step leaves,

$$\begin{aligned} p(\sigma^2 | \mathbf{Y}, \mathbf{W}, \boldsymbol{\tau}, \boldsymbol{\omega}, \lambda_1^2, \lambda_2^2) &\propto \\ &(\sigma^2)^{-(\frac{cn}{2} + \frac{dc}{2} + a_\sigma) - 1} \exp \left\{ -\frac{1}{\sigma^2} \left(\frac{1}{2} \sum_{\ell=1}^n \|\mathbf{y}_\ell - \mathbf{W}^T \mathbf{x}_\ell\|_2^2 + \frac{1}{2} \sum_{i=1}^d \frac{\sum_{j=1}^c w_{ij}^2}{\left(\frac{1}{\tau_{k(i)}^2} + \frac{1}{\omega_i^2} \right)^{-1}} + b_\sigma \right) \right\}, \end{aligned}$$

so that

$$\sigma^2 | \mathbf{Y}, \mathbf{W}, \boldsymbol{\tau}, \boldsymbol{\omega}, \lambda_1^2, \lambda_2^2 \sim \text{Inv-Gamma}(a_\sigma^*, b_\sigma^*),$$

$$\text{where } a_\sigma^* = \left(\frac{cn}{2} + \frac{dc}{2} + a_\sigma \right), \quad b_\sigma^* = \left(\frac{1}{2} \sum_{\ell=1}^n \|\mathbf{y}_\ell - \mathbf{W}^T \mathbf{x}_\ell\|_2^2 + \frac{1}{2} \sum_{i=1}^d \frac{\sum_{j=1}^c w_{ij}^2}{\left(\frac{1}{\tau_{k(i)}^2} + \frac{1}{\omega_i^2} \right)^{-1}} + b_\sigma \right).$$

Full Conditional of $\boldsymbol{\omega}^2, \boldsymbol{\tau}^2$

We consider a joint update of the scale mixing variable based on the corresponding full conditional distribution. We have $p(\boldsymbol{\tau}^2, \boldsymbol{\omega}^2 | \mathbf{Y}, \mathbf{W}, \sigma^2, \lambda_2^2, \lambda_1^2)$

$$\begin{aligned}
& \propto \prod_{k=1}^K \left[\prod_{i \in \pi_k} \left[\left(\sigma^2 \left(\frac{1}{\tau_k^2} + \frac{1}{\omega_i^2} \right)^{-1} \right)^{-\frac{c}{2}} \right] \exp \left\{ - \sum_{i \in \pi_k} \left(\frac{\sum_{j=1}^c w_{ij}^2}{2 \sigma^2 \left(\frac{1}{\tau_k^2} + \frac{1}{\omega_i^2} \right)^{-1}} \right) \right\} \right] \\
& \times \prod_{k=1}^K \left(\frac{\lambda_1^2}{2} \right)^{\left(\frac{m_k c + 1}{2} \right)} (\tau_k^2)^{\left(\frac{m_k c + 1}{2} \right) - 1} \exp \left\{ - \left(\frac{\lambda_1^2}{2} \right) \tau_k^2 \right\} \\
& \times \left[\prod_{i \in \pi_k} \left(\frac{\lambda_2^2}{2} \right)^{\left(\frac{c+1}{2} \right)} (\omega_i^2)^{\left(\frac{c+1}{2} \right) - 1} \exp \left\{ - \left(\frac{\lambda_2^2}{2} \right) \omega_i^2 \right\} (\tau_k^2 + \omega_i^2)^{-\frac{c}{2}} \right]. \\
& \propto \prod_{k=1}^K (\tau_k^2)^{-\frac{1}{2}} \exp \left\{ - \left(\frac{\lambda_1^2}{2} \right) \tau_k^2 - \frac{\|\mathbf{W}^{(k)}\|_2^2}{\tau_k^2 2 \sigma^2} \right\} \\
& \times \prod_{k=1}^K \prod_{i \in \pi_k} (\omega_i^2)^{-\frac{1}{2}} \exp \left\{ - \left(\frac{\lambda_2^2}{2} \right) \omega_i^2 - \frac{\|\mathbf{w}^i\|_2^2}{\omega_i^2 2 \sigma^2} \right\}
\end{aligned}$$

where \mathbf{w}^i denotes the i^{th} row of \mathbf{W} . The above expression shows that the scale mixing variables are conditionally independent given $\mathbf{Y}, \mathbf{W}, \sigma^2, \lambda_2^2, \lambda_1^2$. We next apply a transformation of variables $\nu_k = (\tau_k^2)^{-1}$, Jacobian = $\left| \frac{d}{d\nu_k} \tau_k^2(\nu_k) \right| = \nu_k^{-2}$; $\eta_i = (\omega_i^2)^{-1}$, Jacobian = $\left| \frac{d}{d\eta_i} \omega_i^2 \right| = \eta_i^{-2}$ which yields $p(\boldsymbol{\nu}, \boldsymbol{\eta} | \mathbf{Y}, \mathbf{W}, \sigma^2, \lambda_2^2, \lambda_1^2)$

$$\propto \prod_{k=1}^K (\nu_k)^{-\frac{3}{2}} \exp \left\{ - \left(\frac{\lambda_1^2}{2\nu_k} \right) - \frac{\nu_k \|\mathbf{W}^{(k)}\|_2^2}{2\sigma^2} \right\} \times \prod_{k=1}^K \prod_{i \in \pi_k} (\eta_i)^{-\frac{3}{2}} \exp \left\{ - \left(\frac{\lambda_2^2}{2\eta_i} \right) - \frac{\eta_i \|\mathbf{w}^i\|_2^2}{2\sigma^2} \right\}$$

and from this we see that the conditional distributions lie within the Inverse Gaussian family. More specifically we have

$$\nu_k = \frac{1}{\tau_k^2} \mid \mathbf{Y}, \mathbf{W}, \sigma^2, \lambda_1^2, \lambda_2^2 \stackrel{\text{ind}}{\sim} \text{Inverse-Gaussian} \left(\sqrt{\frac{\lambda_1^2 \sigma^2}{\|\mathbf{W}^{(k)}\|_2^2}}, \lambda_1^2 \right), \quad k = 1, \dots, K$$

independent of

$$\eta_i = \frac{1}{\omega_i^2} \mid \mathbf{Y}, \mathbf{W}, \sigma^2, \lambda_1^2, \lambda_2^2 \sim \text{Inverse-Gaussian} \left(\sqrt{\frac{\lambda_2^2 \sigma^2}{\|\mathbf{w}^i\|_2^2}}, \lambda_2^2 \right), \quad i = 1, \dots, d.$$

2 Supplementary Figures and Tables

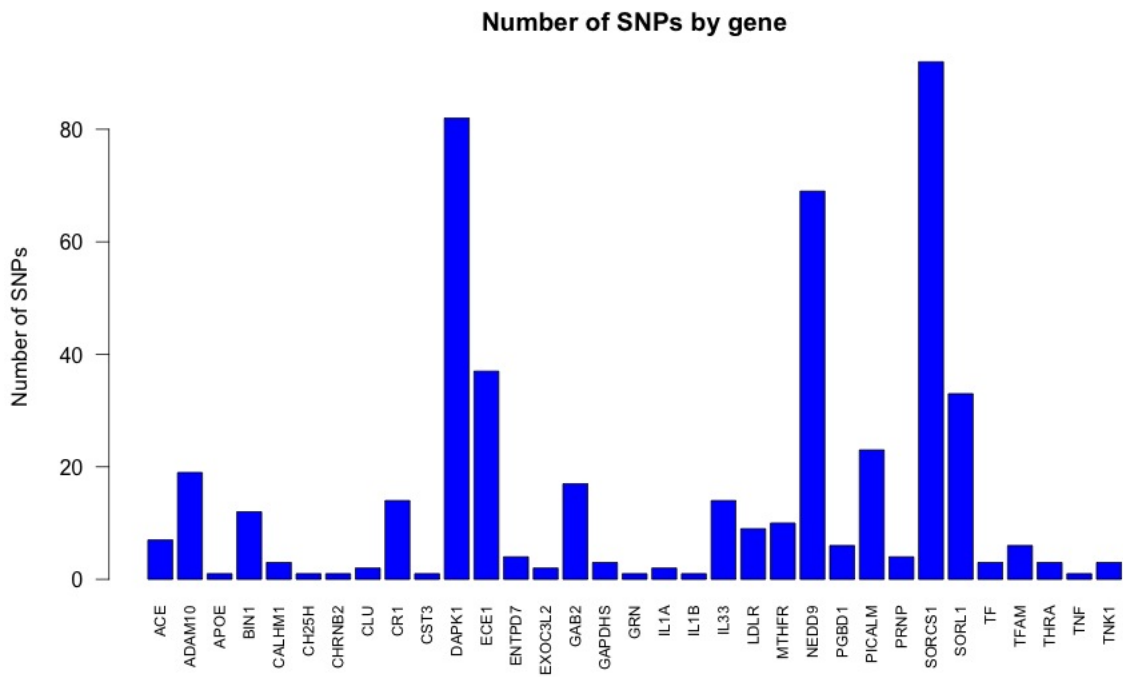


Figure S1: Each of the 33 genes partitioning the 486 SNPs included in the simulation studies and data analysis.

SNP rs405509 from gene APOE

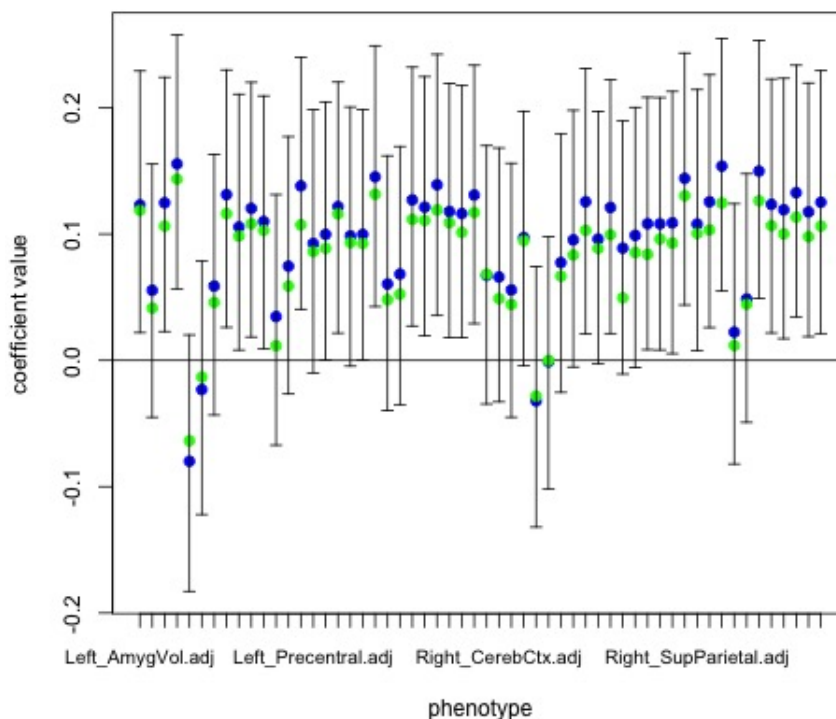


Figure S2: Analysis of the ADNI data: The 95% equal-tail credible intervals relating the SNP rs405509 from APOE to each of the $c = 56$ imaging phenotypes along with the posterior mean estimate (blue) and the Wang et al. (2012) estimate (green). The imaging measures are represented on the x-axis in the same order as they are listed in the rows of Table 2, first for the left hemisphere followed by the right hemisphere.

Table S1: Analysis of ADNI Data - SNP-ROI regression coefficients with 95% equal-tail credible interval excluding the value 0.

SNP	Gene	ROI	Posterior.Mean	X95..CI.Lower	X95..CI.Upper	Wang et al. Estimate
rs405509	APOE	Left AmygVol	0.123	0.022	0.229	0.119
rs2327389	NEDD9	Left AmygVol	0.189	0.004	0.383	0.080
rs10787010	SORCS1	Left AmygVol	-0.127	-0.240	-0.014	-0.120
rs1473180	DAPK1	Left CerebCtx	-0.198	-0.340	-0.055	-0.168
rs1433099	LDLR	Left CerebCtx	0.212	0.058	0.365	0.182
rs12209631	NEDD9	Left CerebCtx	0.165	0.020	0.318	0.092
rs1269918	SORCS1	Left CerebCtx	0.155	0.026	0.286	0.118
rs405509	APOE	Left CerebWM	0.125	0.023	0.224	0.106
rs11601726	GAB2	Left CerebWM	0.145	0.004	0.287	0.077
rs2569537	LDLR	Left CerebWM	-0.173	-0.316	-0.032	-0.103
rs1269918	SORCS1	Left CerebWM	0.158	0.031	0.293	0.118
rs2418811	SORCS1	Left CerebWM	0.201	0.020	0.380	0.127
rs4935774	SORL1	Left CerebWM	-0.148	-0.265	-0.032	-0.114
rs405509	APOE	Left HippVol	0.156	0.057	0.258	0.144
rs12209631	NEDD9	Left HippVol	0.168	0.019	0.311	0.104
rs2756271	PRNP	Left HippVol	0.121	0.013	0.230	0.102
rs10787010	SORCS1	Left HippVol	-0.135	-0.250	-0.021	-0.123
rs10787010	SORCS1	Left InfLatVent	0.126	0.014	0.242	0.105
rs1269918	SORCS1	Left InfLatVent	-0.133	-0.264	-0.003	-0.085
rs2418811	SORCS1	Left InfLatVent	-0.192	-0.375	-0.008	-0.116

rs11601726	GAB2	Left LatVent	-0.155	-0.299	-0.021	-0.072
rs11191692	CALHM1	Left EntCtx	-0.108	-0.218	-0.001	-0.071
rs1473180	DAPK1	Left EntCtx	-0.191	-0.335	-0.049	-0.132
rs2756271	PRNP	Left EntCtx	0.155	0.041	0.268	0.124
rs10787010	SORCS1	Left EntCtx	-0.131	-0.244	-0.020	-0.110
rs10787011	SORCS1	Left EntCtx	-0.148	-0.288	-0.008	-0.081
rs405509	APOE	Left Fusiform	0.131	0.026	0.230	0.116
rs1473180	DAPK1	Left Fusiform	-0.156	-0.300	-0.015	-0.107
rs10787010	SORCS1	Left Fusiform	-0.152	-0.263	-0.041	-0.129
rs4311	ACE	Left InfParietal	-0.212	-0.366	-0.056	-0.160
rs405509	APOE	Left InfParietal	0.106	0.008	0.211	0.098
rs405509	APOE	Left InfTemporal	0.120	0.018	0.220	0.108
rs2756271	PRNP	Left InfTemporal	0.114	0.002	0.225	0.099
rs10787010	SORCS1	Left InfTemporal	-0.114	-0.228	-0.002	-0.104
rs666004	SORL1	Left InfTemporal	0.208	0.018	0.395	0.136
rs405509	APOE	Left MidTemporal	0.110	0.009	0.209	0.103
rs6107516	PRNP	Left MidTemporal	0.141	0.019	0.263	0.109
rs9314349	CLU	Left Parahipp	-0.095	-0.187	-0.003	-0.049
rs6584307	ENTPD7	Left Parahipp	0.148	0.010	0.289	0.088
rs1475345	NEDD9	Left Parahipp	-0.185	-0.344	-0.033	-0.104
rs2756271	PRNP	Left Parahipp	0.112	0.004	0.224	0.085
rs1473180	DAPK1	Left PostCing	-0.169	-0.312	-0.029	-0.140
rs16924159	IL33	Left PostCing	0.174	0.015	0.340	0.160
rs405509	APOE	Left Postcentral	0.138	0.041	0.240	0.107
rs2149196	SORCS1	Left Postcentral	-0.262	-0.477	-0.049	-0.174
rs1023024	SORCS1	Left Precentral	0.182	0.009	0.366	0.088
rs10787010	SORCS1	Left Precentral	-0.117	-0.230	-0.006	-0.103
rs1568400	THRA	Left Precentral	0.111	0.009	0.214	0.092
rs7219773	TNK1	Left Precentral	0.114	0.022	0.207	0.082
rs4311	ACE	Left Precuneus	-0.237	-0.398	-0.079	-0.185
rs405509	APOE	Left Precuneus	0.100	0.000	0.205	0.089
rs1433099	LDLR	Left Precuneus	0.173	0.021	0.328	0.156
rs1699105	SORL1	Left Precuneus	-0.156	-0.304	-0.003	-0.103
rs405509	APOE	Left SupFrontal	0.122	0.022	0.220	0.116
rs744970	NEDD9	Left SupFrontal	0.142	0.001	0.285	0.098
rs4311	ACE	Left SupParietal	-0.235	-0.391	-0.076	-0.178
rs1556758	SORCS1	Left SupParietal	-0.240	-0.465	-0.007	-0.156
rs4311	ACE	Left SupTemporal	-0.210	-0.366	-0.057	-0.142
rs405509	APOE	Left SupTemporal	0.100	0.000	0.199	0.093
rs405509	APOE	Left Supramarg	0.145	0.043	0.249	0.132
rs17496723	NEDD9	Left Supramarg	0.193	0.013	0.378	0.154
rs16924159	IL33	Left MeanCing	0.184	0.024	0.346	0.149
rs10502262	SORL1	Left MeanCing	0.205	0.014	0.395	0.130
rs1699105	SORL1	Left MeanCing	-0.156	-0.304	-0.010	-0.095
rs405509	APOE	Left MeanFront	0.127	0.027	0.232	0.112
rs744970	NEDD9	Left MeanFront	0.154	0.012	0.296	0.102
rs10787010	SORCS1	Left MeanFront	-0.112	-0.224	-0.003	-0.100
rs405509	APOE	Left MeanLatTemp	0.121	0.019	0.225	0.111
rs405509	APOE	Left MeanMedTemp	0.139	0.036	0.242	0.119
rs1473180	DAPK1	Left MeanMedTemp	-0.193	-0.337	-0.049	-0.142
rs10787010	SORCS1	Left MeanMedTemp	-0.172	-0.284	-0.057	-0.153
rs4311	ACE	Left MeanPar	-0.220	-0.383	-0.064	-0.171
rs405509	APOE	Left MeanPar	0.118	0.018	0.219	0.109
rs405509	APOE	Left MeanSensMotor	0.116	0.018	0.218	0.101
rs1023024	SORCS1	Left MeanSensMotor	0.183	0.007	0.359	0.087
rs2149196	SORCS1	Left MeanSensMotor	-0.221	-0.445	-0.003	-0.125
rs7219773	TNK1	Left MeanSensMotor	0.093	0.000	0.186	0.067
rs405509	APOE	Left MeanTemp	0.131	0.029	0.234	0.117
rs1473180	DAPK1	Left MeanTemp	-0.154	-0.299	-0.009	-0.114
rs10787010	SORCS1	Left MeanTemp	-0.141	-0.254	-0.029	-0.125
rs4311	ACE	Right CerebCtx	-0.172	-0.324	-0.016	-0.139
rs11141918	DAPK1	Right CerebCtx	-0.194	-0.381	-0.009	-0.096
rs1473180	DAPK1	Right CerebCtx	-0.160	-0.302	-0.015	-0.146
rs2025935	CR1	Right CerebWM	-0.152	-0.290	-0.013	-0.139
rs16924159	IL33	Right CerebWM	-0.164	-0.334	-0.002	-0.117
rs2569537	LDLR	Right CerebWM	-0.152	-0.294	-0.011	-0.096
rs2418811	SORCS1	Right CerebWM	0.198	0.020	0.379	0.128
rs4935774	SORL1	Right CerebWM	-0.180	-0.296	-0.064	-0.134
rs12209631	NEDD9	Right HippVol	0.157	0.013	0.301	0.086
rs7938033	PICALM	Right HippVol	-0.167	-0.330	-0.002	-0.125
rs2756271	PRNP	Right HippVol	0.126	0.017	0.242	0.111
rs10787010	SORCS1	Right HippVol	-0.158	-0.274	-0.044	-0.138
rs10787011	SORCS1	Right HippVol	-0.138	-0.273	-0.001	-0.111
rs2025935	CR1	Right InfLatVent	0.199	0.060	0.341	0.155
rs3095747	DAPK1	Right InfLatVent	-0.162	-0.289	-0.038	-0.126
rs928413	IL33	Right InfLatVent	-0.134	-0.268	-0.001	-0.055
rs4305	ACE	Right LatVent	0.143	0.009	0.280	0.076
rs7938033	PICALM	Right EntCtx	-0.185	-0.358	-0.019	-0.113
rs10787010	SORCS1	Right EntCtx	-0.125	-0.236	-0.014	-0.106
rs10787011	SORCS1	Right EntCtx	-0.141	-0.282	-0.003	-0.106
rs2025935	CR1	Right Fusiform	-0.144	-0.287	-0.005	-0.121
rs4311	ACE	Right InfParietal	-0.197	-0.356	-0.031	-0.151
rs405509	APOE	Right InfParietal	0.126	0.021	0.231	0.103
rs3118846	DAPK1	Right InfParietal	0.173	0.001	0.349	0.179
rs10502262	SORL1	Right InfTemporal	0.193	0.005	0.378	0.113
rs405509	APOE	Right MidTemporal	0.121	0.021	0.222	0.099
rs6107516	PRNP	Right MidTemporal	0.121	0.000	0.244	0.088

rs4311	ACE	Right PostCing	-0.172	-0.332	-0.015	-0.140
rs17399090	DAPK1	Right PostCing	0.189	0.043	0.338	0.135
rs3124237	DAPK1	Right PostCing	-0.165	-0.332	-0.007	-0.141
rs212539	ECE1	Right PostCing	-0.214	-0.424	-0.009	-0.098
rs12248379	SORCS1	Right PostCing	0.188	0.027	0.362	0.092
rs4311	ACE	Right Postcentral	-0.238	-0.396	-0.080	-0.172
rs405509	APOE	Right Postcentral	0.108	0.008	0.208	0.084
rs4878117	DAPK1	Right Postcentral	-0.134	-0.259	-0.008	-0.080
rs2149196	SORCS1	Right Postcentral	-0.231	-0.448	-0.014	-0.125
rs3744805	THRA	Right Postcentral	0.177	0.051	0.306	0.112
rs7219773	TNK1	Right Postcentral	0.111	0.018	0.204	0.075
rs4311	ACE	Right Precentral	-0.175	-0.330	-0.014	-0.139
rs405509	APOE	Right Precentral	0.108	0.008	0.208	0.096
rs3744805	THRA	Right Precentral	0.166	0.040	0.295	0.112
rs4311	ACE	Right Precuneus	-0.230	-0.386	-0.073	-0.180
rs405509	APOE	Right Precuneus	0.109	0.005	0.213	0.093
rs3811450	CHRNA2	Right Precuneus	-0.133	-0.269	-0.001	-0.115
rs3124237	DAPK1	Right Precuneus	-0.182	-0.342	-0.015	-0.110
rs1433099	LDLR	Right Precuneus	0.159	0.003	0.318	0.139
rs4311	ACE	Right SupFrontal	-0.237	-0.392	-0.081	-0.181
rs405509	APOE	Right SupFrontal	0.144	0.044	0.243	0.130
rs3124237	DAPK1	Right SupFrontal	-0.177	-0.343	-0.014	-0.112
rs4311	ACE	Right SupParietal	-0.254	-0.410	-0.099	-0.191
rs405509	APOE	Right SupParietal	0.108	0.008	0.214	0.101
rs405509	APOE	Right SupTemporal	0.126	0.026	0.226	0.103
rs405509	APOE	Right Supramarg	0.154	0.055	0.255	0.125
rs10502262	SORL1	Right Supramarg	0.193	0.004	0.381	0.117
rs10787010	SORCS1	Right TemporalPole	-0.118	-0.233	-0.001	-0.110
rs1568400	THRA	Right TemporalPole	-0.106	-0.212	-0.004	-0.088
rs17399090	DAPK1	Right MeanCing	0.187	0.038	0.336	0.142
rs4311	ACE	Right MeanFront	-0.200	-0.361	-0.044	-0.156
rs405509	APOE	Right MeanFront	0.150	0.049	0.253	0.126
rs405509	APOE	Right MeanLatTemp	0.124	0.022	0.223	0.107
rs405509	APOE	Right MeanMedTemp	0.119	0.017	0.223	0.100
rs10787010	SORCS1	Right MeanMedTemp	-0.144	-0.263	-0.028	-0.139
rs1699102	SORL1	Right MeanMedTemp	-0.246	-0.481	-0.020	-0.110
rs4311	ACE	Right MeanPar	-0.240	-0.395	-0.082	-0.183
rs405509	APOE	Right MeanPar	0.133	0.035	0.234	0.113
rs4311	ACE	Right MeanSensMotor	-0.210	-0.367	-0.052	-0.161
rs405509	APOE	Right MeanSensMotor	0.118	0.019	0.220	0.098
rs4878117	DAPK1	Right MeanSensMotor	-0.133	-0.261	-0.007	-0.080
rs3744805	THRA	Right MeanSensMotor	0.185	0.058	0.313	0.123
rs4311	ACE	Right MeanTemp	-0.160	-0.316	-0.003	-0.126
rs405509	APOE	Right MeanTemp	0.125	0.021	0.229	0.106
rs1699102	SORL1	Right MeanTemp	-0.245	-0.468	-0.024	-0.117

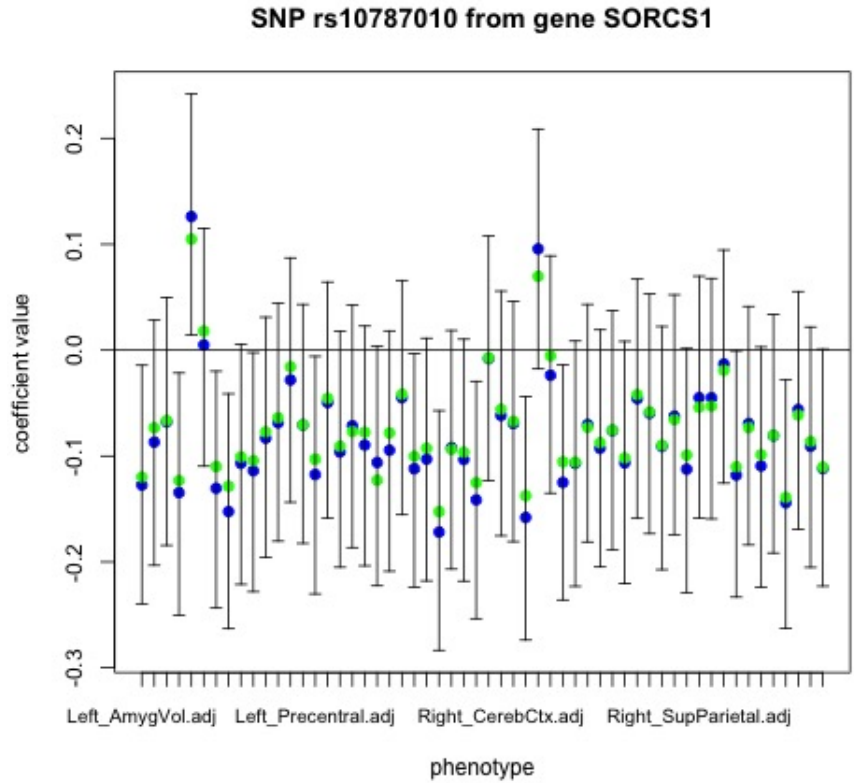


Figure S3: Analysis of the ADNI data: The 95% equal-tail credible intervals relating the SNP rs10787010 from the SORCS1 gene to each of the $c = 56$ imaging phenotypes along with the posterior mean (blue) estimate and the Wang et al. (2012) estimate (green). The imaging measures are represented on the x-axis in the same order as they are listed in the rows of Table 2, first for the left hemisphere followed by the right hemisphere.